Table 1. The primer sets used in this study.

Exon	Direction	Primer sequence (5′-3′)
2	Forward	GCTTGGGAATGTATTGGTCC
2	Reverse	TTCTGGACTCCTCTTTCTGC
3–1	Forward	TTGCTAATGAAGGGGAAAGG
3–1	Reverse	TGAAAGCTGTGATCCTAGTG
4–2	Forward	TACCCAACAGATTCCTATGG
4–2	Reverse	TTGTGGATTCAGAGCTTTGG
4	Forward	TGCTTGGACATGAGCAATAG
4	Reverse	TATTAGGAAGCTCTTTGGGG
5	Forward	GATCTGTAGGGAATGTAGGG
5	Reverse	CAACTGCATCTGAATCAACG
6	Forward	TATTGTGCTTGCTTCCCTTG
6	Reverse	GCAATCAATCTCCTTCTCAG
7	Forward	TACTCTTCCCCATACTTCAG
7	Reverse	CGTTTGGAATGTCTAAGCAG
8	Forward	CCACAGCAAAGTCTCAAATC
8	Reverse	AATAACCCTGTCATGCACAC
9	Forward	CAGTCTCTGTGGTCATTTTG
9	Reverse	TTCATGCTGAGACTGCTCAAG
10	Forward	AAGCCAGCAATGCTTAGTTC
10	Reverse	TGTCACAAGGGAGAACATAC
11	Forward	ATGTGTGCACATACAGAGGT
11	Reverse	GAAGCAAGGACAAGAACCAT
12	Forward	ACCCTTTCCTCTGTGTTTCC
12	Reverse	GCACAATATGCACCAGTGAC
13	Forward	TACTGACCTCAAGTGATCTG
13	Reverse	TTCATTATCTCCTGTGCCTG
14	Forward	CTGTTACATGAACTCCCAAG
14	Reverse	TTGTTGAAAAGCAAGCGAGG
15	Forward	CCATTCGTATGTCCACTATC
15	Reverse	GAGTAGTATCGTATATTCGC
16	Forward	AGTTCTGGAACTCTTTGTTG
16	Reverse	AGAGACAAGTACTCAGGATG
17	Forward	GGTGGATATGCCTGTCTAAG
17	Reverse	AAAGTGCTCAGTTCAGCCTG
18	Forward	GGCTCCTAGGTTATTGAATA
18	Reverse	GTGGTACAAGAAATCTCAAC
19	Forward	TTCTAATGGTGCCTGTGTGC
19	Reverse	CAATGTTAGCCAGAGATCTC
20	Forward	GTGTCAACCTGAAAGAAAAC
20	Reverse	TTTCAGTAAGGAGCCATATC
21	Forward	ATGACCTGGAATGTTCCATC
21	Reverse	GCCTGTTCTTATGTCCTAAC
22	Forward	TATAATGAGCCAGGGTGAAC
22	Reverse	TTTGGAACTGATCATCTGCC
23	Forward	CTTTTCTCTCAACCATCATC
23	Reverse	ACAGTGAATTTGTGGTTCTC
24	Forward	AGCTGGGGCTACAGAGTTTA
24	Reverse	TATCTTGGGAGCGTTCTGAG
25	Forward	GTAACTTTGACTGCTCTGGG
25	Reverse	CGAGCAAGTAGTTGAGTGAG
26	Forward	GGGCTGTGAAATTCTCATTG
26	Reverse	AACTCTGGCATCCCCCATAG
27–1	Forward	CATGTTAGGGGATTGTGAAG
27–1	Reverse	ATACGTTGCCTCACATTCAG
27–2	Forward	CAGAATGGTGAATGCTCTTG
27–2	Reverse	GAAAGGTGAAGACTGTTCTG
27–3	Forward	AAAAAAACCTGTTCCTTCCG
27–3	Reverse	TTTGTCGTTTCCACTGTTAG
27–4	Forward	GAAGAAACTATTTCCCCAAG
27–4	Reverse	GAATATCTGTGCTATGAGAG
27–5	Forward	TAGAGTACAGTTCAATCACG
27–5	Reverse	ATGGATTTCACATTCCTAGG
27–6	Forward	TCTGTGAAGCCAGATCAAAC
27–6	Reverse	GTTTAGATGGCCAAGATGAC

co-localization with mGluR6 [11,19]. *Trpm1* null mutant mice completely lose the photoresponse of ON BCs. Trpm1-L channel activity is negatively regulated by activated G_o in the mGluR6 cascade, and we showed that Trpm1-L is a component of the ON BC transduction channel. Interestingly, the *trpm1*-deficient mice showed similar electrophysiological responses to the responses of those with complete CSNB—significantly reduced b-waves—which led us to examine whether the gene is mutated in human patients with complete CSNB.

Very recently three groups reported the association of TRPM1 mutations with CSNB [20-22]. Independently from these studies, in our present study, we identified five different novel mutations in the human *TRPM1* gene: IVS2–3C>G, IVS8+3_6delAAGT, R624C (c.1870C>T), S882X (c. 2645C>A), and F1075S (c.3224T>C). In addition, our biochemical and cell biologic analyses suggested that the two intron mutations were likely to result in abnormal protein production by abnormal splicing, and the two missense mutations lead to the mislocalization of the TRPM1 protein in BCs. Fundus examination revealed no abnormalities other than myopic changes, and the single bright-flash, mixed rod-cone ERG showed a "negative-type" configuration with a reduced normal a-wave and a significantly reduced b-wave amplitude.

METHODS

Subjects: Four separate patients with complete CSNB (#204, #373, #437, and #484) in whom previous molecular examination revealed no mutation in either *NYX* or *GRM6* among 11 separate patients were analyzed. They were all male, and their ages were 26, 9,19, and 27 years, respectively. They complained of night blindness from early childhood, and otherwise had no health problems. All individuals examined had been under observation at the Department of Ophthalmology of Nagoya University, Nagoya, Japan. The research protocol was designed in compliance with the Declaration of Helsinki and approved by the institutional review board. Written informed consent was obtained from the subjects after an explanation of the purpose of this study was provided. Briefly, the protocol entails molecular analysis of causative genes from blood samples of patients with complete CSNB and in vitro analysis including expression assay and cytological assay using the samples without any disadvantages for the patients.

DNA analysis of patients with complete CSNB: Genomic DNA was extracted from the peripheral blood leukocytes. Exons 2 through 27 of *TRPM1* were amplified by polymerase chain reaction (PCR) using the DNA Thermal Cycler 9700 (Applied Biosystems, Foster City, CA). Primers were designed by and purchased from Invitrogen (Carlsbad, CA). The primer sets used in this study are shown in Table 1. For all exons, 100 ng of genomic DNA was amplified in a 50 µl reaction with 0.5 µM of each primer, 0.2 mM of each dNTP, and Ampli*Taq* Gold polymerase (Applied Biosystems). The

PCR conditions were as follows: 5 min at 94 °C; 35 cycles at 94 °C for 30 s, followed by 30 s at 54 °C, and 45 s at 72 °C; and a final extension step at 72 °C for 7 min. The PCR products were directly sequenced using an ABI PRISM 3100 Genetic Analyzer (Applied Biosystems) and BigDye Terminator v3.1 Cycle Sequencing Kit (Applied Biosystems). To search for polymorphisms, exons 3, 8, 16, 21, and 24 of *TRPM1* from 200 alleles (50 men and 50 women) from unrelated, normal Japanese individuals were directly sequenced.

TRPM1 splicing minigene constructs: DNA fragments of *TRPM1* exon 2 with its downstream splice donor region (nucleotide position in GenBank # NC_000015: 24738–25055; exon 2+SD) and exon 8 with its downstream splice donor region (39020–39392; exon 8+SD) were PCR-amplified using human genomic DNA as a PCR template; SacI and KpnI sites were appended to the 5′ and 3′ ends, respectively. A partial fragment of β-globin (*HBB*) intron 2 (614–1166 in GenBank # NC_000011) was PCR-amplified; KpnI and SalI sites were appended to the 5′ and 3′ ends, respectively. DNA fragments of *TRPM1* exon 3 with its upstream splice acceptor region (31325–31691; SA+exon 3) and exon 9 with its splice acceptor region (39976–40280; SA +exon 9) were PCR-amplified using human genomic DNA as a PCR template; SalI and BamHI sites were appended to the 5′ and 3′ ends, respectively. The exon 2+SD, *HBB* intron, and SA+exon 3 fragments (exon 2+3 construct), or exon 8+SD, *HBB* intron, and SA+exon 9 (exon 8+9 construct) were ligated and subcloned into the SacI and BamHI sites of *pBluescript KS+* (Stratagene), containing three repeats of the Flag-tag between the BamHI and NotI sites. The generated exon 2+3 construct and exon 8+9 construct were digested with SacI and NotI and subcloned into SacI and BamHI digested pEGFP-C3 and pEGFP-C2 (Clontech, Palo Alto, CA), respectively, each with a synthesized BglII-NotI linker.

Transfection and western blots analysis: HEK293T cells were cultured in D-MEM containing 10% fetal bovine serum (FBS; Nissui, Tokyo, Japan). These cells were grown under 5% carbon dioxide at 37 °C. Transfections were performed using the calcium phosphate method. Transfected cells were incubated at 37 °C for 48 h, and harvested for further analysis. Cell extract proteins were separated by SDS–PAGE, and transferred to a polyvinylidene difluoride membrane (ATTO, Tokyo Japan). The membrane was incubated with a mouse anti-Flag antibody (1:1,000; Sigma, St Louis, MO), a rabbit anti-β−gal antibody (1:10,000; Chemicon, Temecula, CA), or a mouse anti-β−actin antibody (1:2,000; Sigma), and incubated with a horseradish peroxidase-conjugated goat anti-mouse or -rabbit IgG (1:10,000; Zymed Laboratories, San Francisco, CA). The bands were visually developed using Chemi-Lumi One L (Nacalai Tesque, Kyoto, Japan).

In vivo electroporation and section immunohistochemistry: In vivo electroporation was performed at postnatal day 0 (P0) as described previously [23]. Approximately 0.3 µl of DNA solution (5 µg/µl) was injected into the subretinal space of P0 mouse pups, and square electric pulses (80 V; five 50 ms pulses with 950 ms intervals) were applied with electrodes. Wild-type (WT) and mutant forms of *TRPM1* (R624C and F1075S) containing 3× Flag at the C-terminus were expressed from the mouse *mGluR6* promoter (mGluR6-TRPM1–3×Flag). To generate this construct, the chicken β-actin gene (CAG) promoter region in *CAG-TRPM1* was replaced with the 9.5 kb fragment of *mGluR6* 5′ upstream genomic sequence [24]. mGluR6-TRPM1–3×Flag (4 µg/µl) and CAG-GFP (1 µg/µl) were co-electroporated and harvested at P14. Immunohistochemistry to observe the subcellular localization of TRPM1–3×Flag expressed in the electroporated ON BCs was performed on sections as previously described [23]. Mouse anti-Flag antibody (1:500), rabbit anti-PKCα antibody (1:20,000; Sigma), and rat anti-GFP antibody (1:1,000; Nacalai Tesque) were used. The signal intensity of Flag immunostaining at the dendritic tips and somas of ON BCs was measured using AxioVision software (Carl Zeiss, Oberkochen, Germany). The ON BCs that showed more intensity in the dendritic tips than in the somas were counted. One hundred electroporated ON BCs were counted from three retinas independently prepared for each construct.

Clinical evaluations in patients associated with TRPM1 mutations: The ophthalmologic examination included best-corrected visual acuity, refraction, biomicroscopy, ophthalmoscopy, fundus photography, Goldmann kinetic perimetry, color vision testing, and electroretinography [25]. Standardized full-field ERGs were elicited by Ganzfeld stimuli after pupillary dilation with 0.5% tropicamide and 0.5% phenylephrine hydrochloride and 20 min of dark-adaptation. The rod (scotopic) ERGs were elicited by a blue stimulus with a luminance of 5.2×10^{-3} cd/sec•m^2. The mixed rod-cone, single flash (bright white) ERGs were elicited by a white stimulus of 44.2 cd/sec•m^2. The photopic (cones) single-flash ERGs and 30 Hz flicker ERGs were elicited by white stimuli at a luminance of 4 cd/sec•m^2 and 0.9 cd/sec•m^2, respectively, on a white background of 68 cd/m^2. The single flash bright white ERGs were recorded again after 17 h of dark adaptation.

ERG recordings in the trpm1 null mutant (trpm1$^{-/-}$) mice: We generated *trpm1*$^{-/-}$ mice as described previously [11]. Our methods for recording the ERGs from the mice have been described in detail [26]. In brief, the mice were dark-adapted overnight, and then anesthetized with an intramuscular injection of 70 mg/kg ketamine and 14 mg/kg xylazine. ERGs were recorded with a gold-wire loop electrode placed on the anesthetized cornea. The mice were placed in a Ganzfeld bowl and stimulated with stroboscopic stimuli of 1.0 log cd-s/m^2 (photopic units) maximum intensity. Four levels of stimulus intensity ranging from −5.0 to 1.0 log cd-s/m^2 were used for the dark-adapted ERG recordings, and four levels of stimulus intensity ranging from −0.5 to 1.0 log cd-s/m^2 were used for the light-adapted ERGs. The light-adapted ERGs were

recorded on a rod-suppressing white background of 1.3 log cd-s/m^2 (photopic units). The amplitude of the a-wave was measured from the baseline to a set time of 8 msec after the initial negative wave for the dark-adapted ERG, and 11 msec for the light-adapted ERG. The b-wave amplitude was measured from the negative trough of the a-wave to the maximal positive peak.

Animal care: All procedures conformed to the ARVO Statement for the Use of Animals in Ophthalmic and Vision Research, and these procedures were approved by the Institutional Safety Committee on Recombinant DNA Experiments and the Animal Research Committee of Osaka Bioscience Institute. The mice were housed in a temperature-controlled room with a 12h:12h light-dark cycle. Fresh water and rodent diet were available at all times.

RESULTS

DNA analysis of the complete CSNB patients: Five different mutations in *TRPM1* were identified: IVS2–3C>G, IVS8+3_6delAAGT, R624C (c.1870C>T), S882X (c. 2645C>A), and F1075S (c.3224T>C). Mutations were present in three unrelated patients with complete CSNB (#373, #437, and #484). All three patients were compound heterozygotes. Their pedigrees and the DNA sequence chromatogram for the patients harboring these mutations are presented in Figure 1A,B.

The two intron changes, IVS2–3C>G and IVS8+3_6delAAGT (Figure 1C), were interpreted to be pathogenic because no RNA splicing activities were detected when each of the two changes was present (see splicing assay section). They were also predicted to affect RNA splicing, as assessed by an online splice-site prediction tool. The donor site prediction score from the software for the exon 8 donor site in *TRPM1* was 0.99 for the WT sequence, whereas it was under 0.01 for the corresponding mutated sequence with the IVS8+3_6delAAGT sequence change. The acceptor site prediction score for the exon 3 acceptor site in *TRPM1* was 0.98 for the WT sequence, whereas it was 0.44 for the mutated sequence with the IVS2–3C>G sequence change. The two mutations were not found in an analysis of 100 Japanese normal controls.

The S882X mutation was considered to be a pathogenic null mutation since mRNA containing the predicted early stop codon would most likely be subject to nonsense mediated decay without being translated into a protein [27]. Even if the translated protein was produced, it would lack the C-terminus region of TRPM1, including transmembrane domains 4–6, which is very likely to lead to a loss of function as a cation channel (Figure 1D). This change was not found among the 100 healthy control individuals we examined. The two missense changes in the *TRPM1* gene, R624C and F1075S, were located in the N-terminal region and in the C-terminal end of the transmembrane domain, respectively (Figure 1D). They were interpreted as likely pathogenic because the arginine at position 624 and the phenylalanine at 1075 are well conserved among the TRPM subfamily, suggesting the importance of these amino acid residues for TRPM function (Figure 1E). The two mutations were not found in an analysis of 100 Japanese normal controls. None of the five mutations mentioned above have been reported in a SNP database.

Analysis of protein expression from TRPM1 mutant minigenes: Our previous expression analysis of mouse TRPM1 showed that the long form (TRPM1-L), which functions as a cation channel, is predominantly expressed in the retina [11], suggesting that human patient samples for directly analyzing splicing are not readily available. To overcome this limitation, minigenes for expression in tissue culture cells were designed; these minigenes included the upstream exons (exon 2 or 8) fused with EGFP, downstream exons (exon 3 or 9) fused with 3×Flag-tags, and a *HBB* intron, which is often used in splicing assays (an exon 2+3 minigene and an exon 8+9 minigene; Figure 2A). Since the signals required for constitutive splicing are usually within ~100 nucleotides of splice junctions [11], we took ~200 nucleotide regions for both splicing donors and acceptors to ensure the splicing assay. We also generated mutated minigenes containing the IVS2–3C>G mutation in the exon 2+3 minigene or the IVS8+3_6delAAGT mutation in the exon 8+9 minigene. Minigene splicing was analyzed in HEK293T cells since they have been used extensively to study constitutive RNA splicing. HEK293T cells were transfected with minigene DNA and a lacZ expression internal control vector, and western blotting was performed on whole cell extracts isolated 48 h later. We then analyzed protein products of the EGFP-exon 2+3 fusion and the EGFP-exon 8+9 fusion proteins by western blot analysis of whole cell extracts transfected with the WT and mutated minigenes. We detected an expected 45 kDa or 39 kDa band with the anti-Flag antibody in HEK293T cell extracts transfected with the WT exon 2+3 minigene or the exon 8+9 minigene (Figure 2B,C). In contrast, we did not detect any bands in either of the cell extracts transfected with the mutated minigenes. We detected the β-gal bands of the transfection internal control, and the β-actin bands of the cell extract control in both the WT and mutant minigene transfected cells. These results showed that both the IVS2–3C>G and IVS8+3_6delAAGT mutations abrogate normal splicing and lead to abnormal protein production, suggesting that these *trpm1* alleles are loss-of-function alleles.

In vivo analysis of intracellular localization of TRPM1 protein carrying missense mutations: The TRPM1 missense mutations R624C and F1075S are located in the N-terminal and the C-terminal end of the six-transmembrane domains (6TM), respectively (Figure 1D). Mutations in these regions often cause misfolding/mislocalization of the protein, and/or a defect in channel activity [28-32]. To determine the

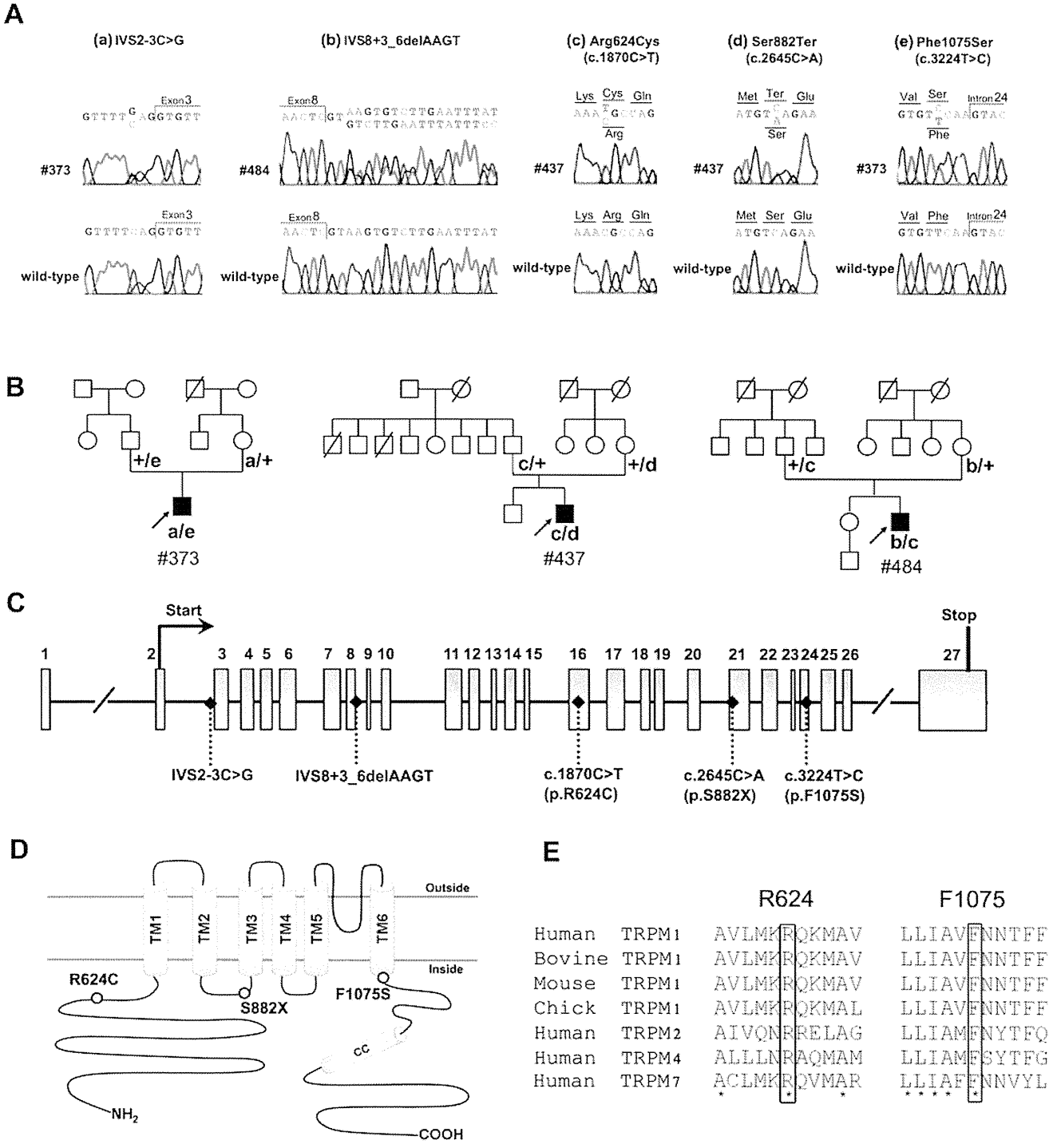

Figure 1. Compound heterozygous *TRPM1* mutations identified in patients #373, #437, and #484. **A**: Sequence chromatograms showing the mutations: IVS2–3C>G in patient #373 (a), IVS8+3_6delAAGT in patient #484 (b), Arg624Cys (c. 1870C>T) in patients #437 and #484 (c), Ser882Ter (c. 2645C>A) in patient #437 (d), and Phe1075Ser (c. 3224T>C) in patient #373(e). **B**: Complete CSNB pedigrees of Japanese patients #373, #437, and #484. These three patients are compound heterozygotes of *TRPM1* mutations. **C**: Exon structures of human *TRPM1*. The first methionine (Start) and a stop codon (Stop) of the *TRPM1* open reading frame are indicated. All mutations found in this study are shown. **D**: Putative topology of the human TRPM1. All mutations found in this study are illustrated. The six transmembrane domains are indicated as TM1-TM6. **E**: Alignment of R624 and F1075 in TRPM proteins. Sequence alignment of TRPM1 from human, bovine, mouse, chick, and TRPM2, TRPM4, and TRPM7 from human. Amino acid residues R624 and F1075 are boxed. The asterisks indicate completely conserved residues.

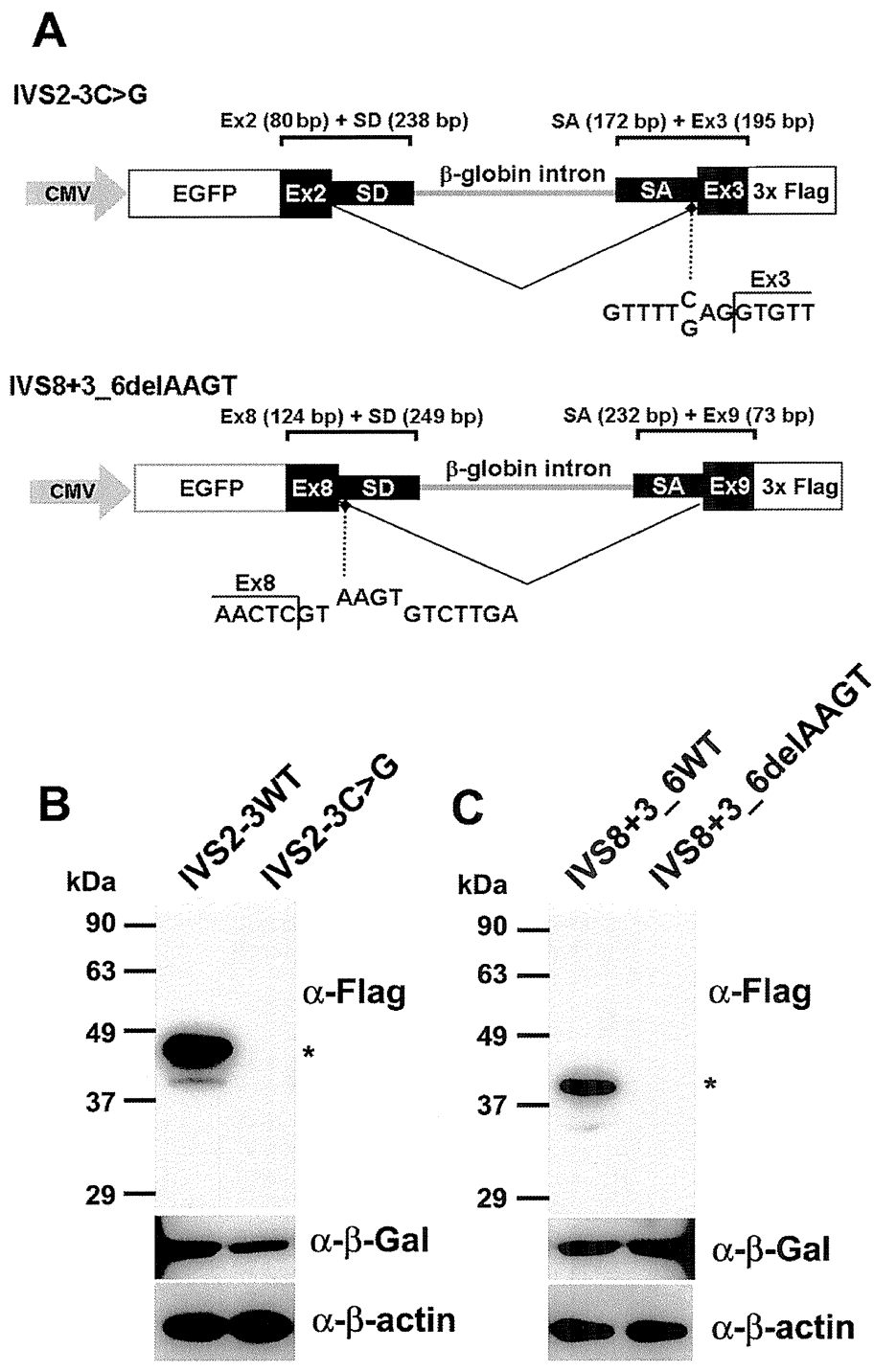

Figure 2. Analysis of protein expression from *TRPM1* mutant minigenes. **A**: Schematic of *TRPM1* minigenes. The minigene *IVS2–3C>G* contains an *EGFP* gene, exon 2, the exon 2 splice donor region, a portion of the β-globin (*HBB*) intron 2, the exon 3 splice acceptor region, and exon 3, and uses the *CMV* promoter and *SV40 polyA* site from the *pEGFP-C3* vector. The minigene IVS8+3_6delAAGT contains an *EGFP* gene, exon 8, the exon 8 splice donor region, a portion of the *HBB* intron 2, the exon 9 splice acceptor region, and exon 9, and uses the CMV promoter and *SV40 polyA* site from the *pEGFP-C2* vector. Mutations of IVS2–3C>G and IVS8+3_6delAAGT are shown. **B-C**: western blots of HEK293 cell extracts transfected with minigenes IVS2–3C>G (**B**) or IVS8+3_6delAAGT (**C**). WT represents protein from a wild-type minigene transfection, and asterisks represent spliced EGFP detected by an anti-Flag antibody. β-Gal and β-actin were used for transfection control and loading control, respectively.

functional relevance of R624C and F1075S TRPM1 residues, we mutagenized the *TRPM1* cDNA to introduce R624C and F1075S mutations. We first prepared expression vectors encoding R624C or F1075S mutant proteins attached with a Flag-tag at the C-terminus, and expressed them both, as well as WT vectors, in HEK293T cells. We did not observe a significant difference in the protein level between the mutants and WT by western blotting, suggesting that the protein stability of R624C and F1075S was not affected (data not shown). We then prepared expression vectors of *R624C-* and *F1075S-TRPM1* cDNAs fused with the mouse *mGluR6* 9.5 kb promoter that drives ON BC-specific expression (Figure 3A). We electroporated each of them as well as the WT vector into the P0 mouse retinas. We examined the localization of the

expressed TRPM1 mutant proteins in ON BCs at P14 when the endogenous mouse TRPM1 is preferentially localized to the dendritic tips [11,19]. The electroporated human TRPM1 was visualized by an anti-Flag tag antibody. TRPM1 WT was localized at the soma (arrow) and dendritic tips (arrowheads) of the ON BCs (Figure 3B,C). On the other hand, the immunostaining signals of both the R624C and the F1075S TRPM1 proteins were significantly weaker than those of the WT protein (Figure 3D-G). We quantified the number of electroporated ON BCs in which the WT TRPM1 protein was localized more in the dendritic tips than somas. About 70% of ON BCs that electroporated with WT TRPM1 showed a brighter TRPM1 signal at the dendritic tips, and the signals on the dendritic tips were dramatically reduced in both mutant proteins (Figure 3H). These results may imply that R624C and F1075S mutations lead to mislocalization of TRPM1 protein and are responsible for the protein trafficking of TRPM1 channel proteins. However, it should be noted that there is also a possibility that the transfected TRPM1 proteins are misfolded due to the addition of the 3xFlag tag, leading to the undetectability of Flag-tagged mutant proteins specifically in the dendrites. Future analysis is required to obtain a conclusive result on this point.

Clinical characteristics of the complete CSNB patients associated with TRPM1 mutations: The clinical characteristics of the three complete CSNB patients with *TRPM1* mutations are summarized in Table 2. All the patients showed the typical clinical features of complete CSNB. They complained of night blindness from their early childhood, and the best-corrected visual acuities were normal in two patients (#373 and #437) and mildly reduced in one (#484). The refractive errors were highly or moderately myopic, and astigmatism was present in all of the patients (Table 2). Mild nystagmus and esotropia was observed in the patient with reduced visual acuity (#484). Slit lamp examination revealed no abnormality, and all fundus examinations revealed no abnormalities in the posterior pole other than myopic changes, including the tilted discs and temporal pallor of the optic discs (Figure 4). Goldmann kinetic visual fields and color vision tests with the Ishihara plates, the AO H-R-R pseudoisochromatic plates, and Farnsworth D-15 panel test were conducted in two patients (#437 and #484) with normal results. No family history was obtained from the patients (Figure 1B).

The full-field scotopic (rod) ERGs elicited by a blue light were non-recordable after 20 min of dark-adaptation (Figure 5B). The photopic ERG showed an a-wave with apparently normal implicit time and a b-wave with delayed implicit time (Figure 5C). The amplitudes of the 30 Hz flicker ERG were within normal range (Figure 5D). The single bright-flash, mixed rod-cone ERG elicited by a white stimulus had a "negative-type" configuration with a reduced normal a-wave and with a significantly reduced b-wave amplitude (Figure 5A). The oscillatory potentials were reduced.

ERG analysis of the trpm1 null mutant (trpm1$^{-/-}$) mice: To address a possible role of TRPM1 in ON BC function, we previously generated *trpm1* null mutant (*trpm1*$^{-/-}$) mice by targeted gene disruption [11]. Next, to compare the physiologic retinal function of *trpm1*$^{-/-}$ between humans and mice, we recorded mouse ERGs in 8-week-old mice (Figure 6). The dark-adapted (rod) ERGs elicited by different stimulus intensities from WT and *trpm1*$^{-/-}$ mice are shown in Figure 6A. The amplitudes of the a-wave, originating from the photoreceptors, were approximately equal for both types of mice (Figure 6B). In contrast, the dark-adapted ERG b-wave, originating mainly from the ON BCs, in *trpm1*$^{-/-}$ mice was not present at the lower intensities, and only a very small positive inflection was seen at the highest stimulus intensity of 1.0 log cd-s/m^2 (Figure 6C). The ERGs elicited by different stimulus intensities from light-adapted WT and *trpm1*$^{-/-}$ mice are shown in Figure 6D. The b-wave was severely depressed or absent leaving only the a-wave in the *trpm1*$^{-/-}$ mouse (Figure 6E,F). These ERG results are similar to those obtained by other groups [19,33], and suggested that the function of both rod and cone ON BCs, and the signal transmission from rod and cone photoreceptors to BCs were severely impaired in *trpm1*$^{-/-}$ mice. In contrast, the presence of a normal a-wave indicated that the rod and cone photoreceptors were functioning normally in this mutant mouse.

DISCUSSION

An essential step in intricate visual processing is the segregation of visual signals into ON and OFF pathways by retinal BCs [34]. The release of glutamate from photoreceptors modulates the photoresponse of ON BCs [35] via metabotropic glutamate receptor 6 (mGluR6) and the G-protein (G_o) that regulates a cation channel [36-38]. We recently reported that we identified a mouse *trpm1* long form (*trpm1-L*) and found that TRPM1-L localization is developmentally restricted to the dendritic tips of ON BCs in co-localization with mGluR6 [11]. *Trpm1* null mutant mice completely lose the photoresponse of ON BCs. TRPM1-L channel activity is negatively regulated by activated G_o in the mGluR6 cascade. These results suggest that TRPM1-L is a component of the ON BC transduction channel. These observations led us to examine whether the gene is mutated in human patients with complete CSNB in the current study.

To identify human *TRPM1* gene mutations in CSNB patients, we analyzed four separate Japanese patients with complete CSNB in whom previous molecular examination revealed no mutation in either the *NYX* or *GRM6* genes. In the current study, we identified five different mutations in *TRPM1*: IVS2–3C>G, IVS8+3_6delAAGT, R624C (c. 1870C>T), S882X (c.2645C>A), and F1075S (c.3224T>C). Mutations were present in three unrelated patients with complete CSNB (#373, #437, and #484). Using a minigene expression assay, we showed that two intron mutations,

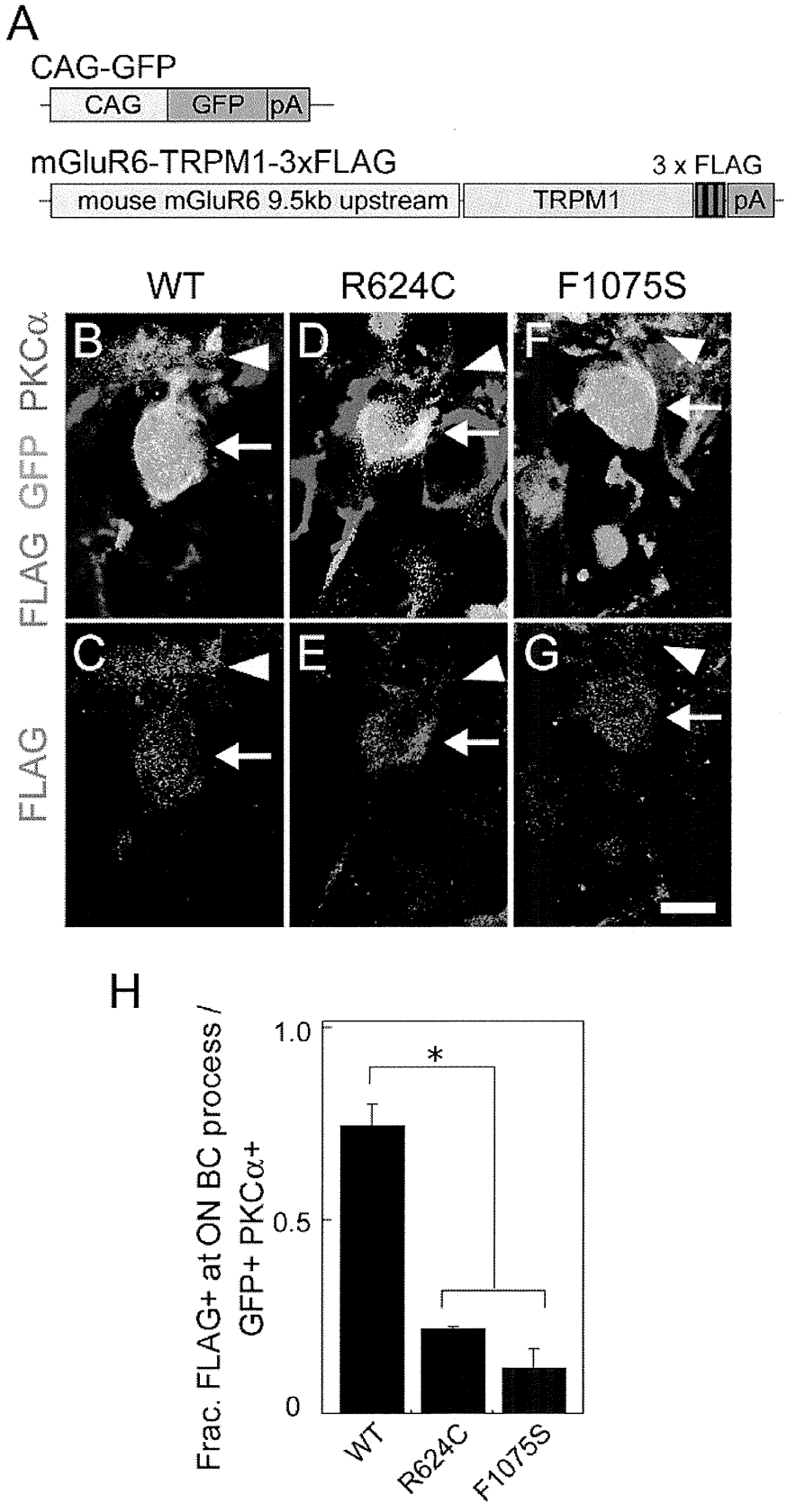

Figure 3. In vivo electroporation of WT, R624C, and F1075S *TRPM1* expression vectors fused with the *mGluR6* promoter. **A**: DNA constructs used for electroporation. *CAG-GFP* was co-electroporated to identify electroporated regions. WT and mutant forms of *TRPM1* fused with *3×Flag* were expressed under the mouse *mGluR6* 9.5 kb promoter. **B-G**: Section immunohistochemistry of the P14 retinas electroporated in vivo at P0 with *CAG-GFP* and *mGluR6-TRPM1–3×Flag*. The sections were immunostained with PKCα (blue), GFP (green), and Flag (red) antibodies (**B**, **D**, and **F**). Immunostaining with Flag was visualized separately (**C, E** and **G**). Arrows represent the soma and arrowheads represent the dendritic tips of ON BC. Scale bar: 10 μm. **H.** Composition of electroporated ON BC (GFP+ PKCα+), where bright Flag signal was observed in the dendrites. The error bars represent standard deviation (SD). Asterisks show that the differences are statistically significant (n=3) (Student's *t*-test, $p<0.05$).

Table 2. Clinical Characteristics in complete CSNB with TRPM1 mutations.

Mutation	Corrected visual acuity	Refraction	Color vision	Fundus appearance	Visual field	Night blindness	Nystagmus	Strabismus
patient #373 (Male, 9 years old)								
IVS3–3C>G, F1075S	1.0 (OD)	−8.25 −2.75 X 40 (OD)	ND	Myopic	ND	+	−	Orthophoria
	1.0 (OS)	−8.25 −0.50 X 180 (OS)						
patient #437 (Male, 19 years old)								
R624C, S882X	1.0 (OD)	−4.50 −2.25 X 120 (OD)	Normal	Myopic	Normal	+	−	Orthophoria
	1.0 (OS)	−4.50 −2.75 X 50 (OS)						
patient #484 (Male, 27 years old)								
IVS9+3_6delA AGT, R624C	0.5 (OD)	−13.00 −3.00 X 90 (OD)	Normal	Myopic	Normal	+	+	Esotropia

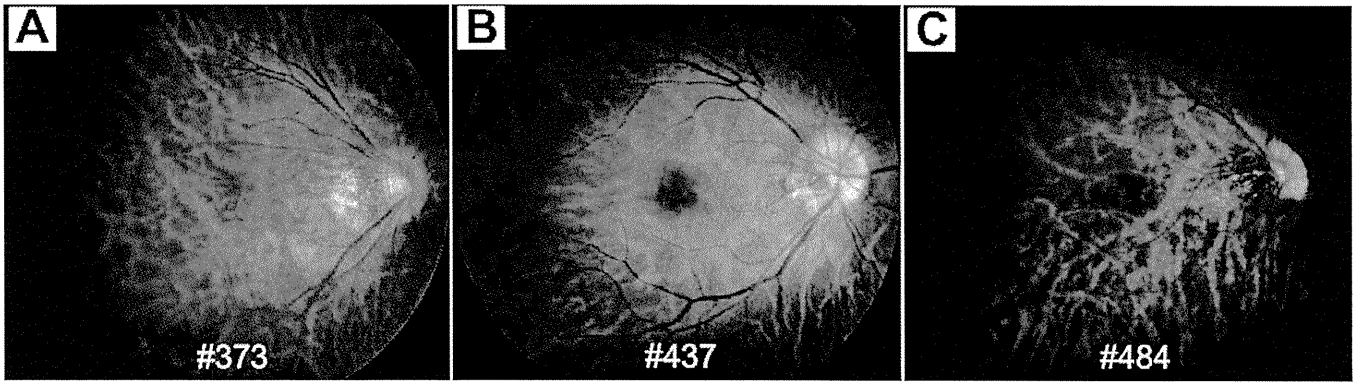

Figure 4. Fundus photographs of patients with mutations of *TRPM1*. **A-C**: Fundus images of patient #373 (**A**), patient #437 (**B**), and patient #484 (**C**). All fundus examinations revealed no abnormalities in the posterior pole other than myopic changes, including the tilted discs and temporal pallor of the optic discs. The patient's number is indicated in each photograph.

IVS2–3C> and IVS8+3_6delAAGT, can cause splicing abnormalities leading to defects in protein production. Since these two mutations are located in the N-terminus region of TRPM1, these mutations are likely to produce a loss-of-function allele of *TRPM1*. The nonsense mutation S882X (c. 2645C>A) is located between TM2 and TM3. Thus, the truncated TRPM1 protein is likely to be non-functional as a channel. Regarding the two missense mutations, R624C (c. 1870C>T) and F1075S (c.3224T>C), we observed failure of the transportation of the missense mutant channels to the dendritic tips. However, ~20% of ON BCs could transport the mutant forms of TRPM1, suggesting that these ON BCs are still active. Considering that human patients carrying these mutations still have cone ERG responses, this fraction might be cone ON BCs converging inputs from cone photoreceptors. Since these two amino acid residues are evolutionarily conserved among the TRPM subfamily, these amino acid residues are indispensable for the physiologic functions of TRPM channels. For example, R671Q mutation in the *Drosophila TRPM1* homolog (trp^{14}) resulted in a significant reduction of ERG response [39]. This mutation is located between the 6TM and the TRP domain [40], which is close to the F1075 residue of human TRPM1. Although this region is not in the functional domains, it still could be responsible for the physiologic function of the TRPM channel.

The scotopic ERG b-waves recorded using Ganzfeld stimuli were nonrecordable, and the photopic ERG showed normal a-wave amplitude, but the amplitude of the b-wave is reduced or absent in the three affected human individuals. There seems to be no apparent genotype-phenotype correlation in our patients with *TRPM1* mutations. Full-field ERG results showed no detectable post-receptoral ON-pathway function for the three patients. The ERG amplitudes of patient #484 were smaller than those of the other two patients, but the reductions were considered to be due to high myopia (−12 to −13 D) [41] or other unknown reasons. The function of the inner retina was further analyzed using L-M cone ERGs elicited by rectangular, 100–125 msec duration light stimuli under light-adapted conditions in one patient, and as a result, the amplitude of the b-wave at light onset (ON-response) was significantly reduced, but the d-wave amplitude (OFF-response) at light offset was unaffected with normal

Figure 5. Full-field ERGs of patients with mutations of the *TRPM1* gene. **A-D**: Full-field ERGs recorded in a normal subject and three affected individuals. The single bright-flash, mixed rod-cone ERGs showed a "negative-type" configuration with a reduced normal a-wave and a significantly reduced b-wave amplitude (**A**). The scotopic ERGs showed no response after 20 min of dark-adaptation (**B**). The photopic ERGs showed an apparent a-wave with normal implicit time and a b-wave with delayed implicit time (**C**). The amplitudes of the 30 Hz flicker ERGs were within normal range (**D**). The oscillatory potentials were reduced. Arrowheads: stimulus onset. Each patient's number is noted at left.

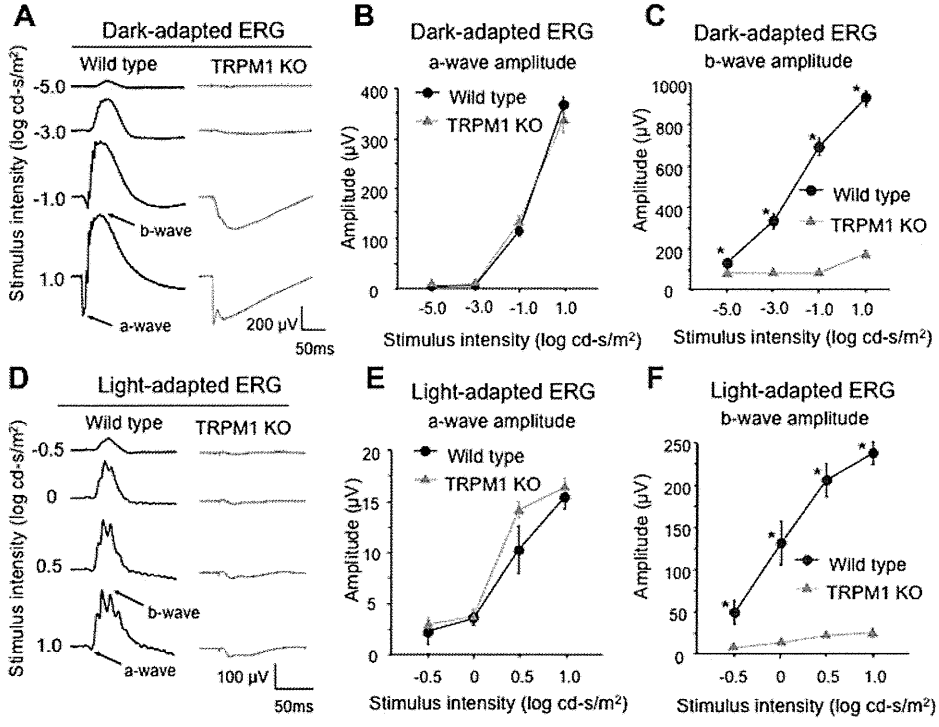

Figure 6. ERG of WT and *trpm1*$^{-/-}$ mice. **A-F**: ERGs recorded from 8-week-old mice. Dark-adapted (**A**) and light-adapted (**D**) ERGs were elicited by four different stimulus intensities in both WT and *trpm1*$^{-/-}$ mice (n=5). Amplitudes of dark-adapted (**B**) and light-adapted (**E**) ERG a-waves as a function of the stimulus intensity are shown. Amplitudes of dark-adapted (**C**) and light-adapted (**F**) ERG b-waves as a function of the stimulus intensity are shown. The bars represent the standard error of the mean (SEM). Asterisks show that the differences are statistically significant (Mann–Whitney test, $p<0.05$). The *trpm1*$^{-/-}$ mouse had a normal a-wave, but a severely depressed b-wave for both dark- and light-adapted ERGs.

OPs on the OFF-responses (data not shown). These electrophysiological results indicated that the pathology in complete CSNB with *TRPM1* mutations lay in the dysfunction of the depolarizing ON BCs because it is generally considered that the positive ON-response (b-wave) reflects the depolarizing ON BCs. The impairment in the ON-response was also observed in the *trpm1*$^{-/-}$ mice in which b-wave amplitude for both scotopic and photopic conditions were completely defective. These results in human and mice strongly indicated that TRPM1 is essential for the function of ON BCs in the visual pathway.

The clinical features of patients with complete CSNB are similar even when the causative gene is different. Most patients complain of night blindness while showing normal fundi accompanied by highly myopic refractive errors [4,5]. The best-corrected visual acuity is mildly reduced, or sometimes normal. We could not clarify any difference in ERG responses that were recorded according to ISCEV

protocol among those with different gene defects. To date, the only phenotypic difference among complete CSNB patients with different gene mutations has been detected using a scotopic 15 Hz-flicker ERG with increasing intensities [42]. It was reported that patients with *TRPM1* mutations showed 15 Hz-flicker ERG responses similar to those with *NYX* mutations, but different from those with *GRM6* mutations or normal control subjects, suggesting some difference in the rod pathway [21].

Very recent studies reported that *TRPM1* gene mutations were the major cause of AR complete CSNB in patients with Caucasian ancestors [20-22]. We previously identified *NYX* mutations in five families and *GRM6* mutations in two families among 11 Japanese families with complete CSNB [43,44], and in the current study, we found *TRPM1* mutations in three of the remaining four families. From these results we confirmed that the gene was responsible for patients with complete CSNB. It is likely that one of the three genes that is localized at the dendritic terminals of ON BCs and contributing the cell activity, *TRPM1*, *GRM6*, or *NYX*, would responsible for most patients with complete CSNB.

In conclusion, we identified five different mutations in the *TRPM1* gene in three unrelated Japanese patients with complete CSNB. *TRPM1* is essential for the depolarizing ON BC function in humans as well as in mice.

ACKNOWLEDGMENTS

We thank S. Nakanishi for providing us the *MG6-Z* vector. We also thank M. Joukan, A. Tani, T. Tsujii, A. Ishimaru, Y. Saioka, K. Sone and S. Kennedy for technical assistance. This work was supported by CREST from Japan Science and Technology Agency, and a Grant for Molecular Brain Science, a Grant-in-Aid for Scientific Research (B) from Ministry of Education, Culture, Sports, Science and Technology, and The Takeda Science Foundation, The Uehara Memorial Foundation, Novartis Foundation, Mochida Memorial Foundation for Medical and Pharmaceutical Research, The Naito Foundation.

REFERENCES

1. Schubert G, Bornschein H. Analysis of the human electroretinogram. Ophthalmologica 1952; 123:396-413. [PMID: 14957416]
2. Carr RE. Congenital stationary nightblindness. Trans Am Ophthalmol Soc 1974; 72:448-87. [PMID: 4376877]
3. Bech-Hansen NT, Naylor MJ, Maybaum TA, Pearce WG, Koop B, Fishman GA, Mets M, Musarella MA, Boycott KM. Loss-of-function mutations in a calcium-channel alpha1-subunit gene in Xp11.23 cause incomplete X-linked congenital stationary night blindness. Nat Genet 1998; 19:264-7. [PMID: 9662400]
4. Miyake Y, Yagasaki K, Horiguchi M, Kawase Y, Kanda T. Congenital stationary night blindness with negative electroretinogram. A new classification. Arch Ophthalmol 1986; 104:1013-20. [PMID: 3488053]
5. Ruether K, Apfelstedt-Sylla E, Zrenner E. Clinical findings in patients with congenital stationary night blindness of the Schubert-Bornschein type. Ger J Ophthalmol 1993; 2:429-35. [PMID: 8312830]
6. Bech-Hansen NT, Naylor MJ, Maybaum TA, Sparkes RL, Koop B, Birch DG, Bergen AA, Prinsen CF, Polomeno RC, Gal A, Drack AV, Musarella MA, Jacobson SG, Young RS, Weleber RG. Mutations in NYX, encoding the leucine-rich proteoglycan nyctalopin, cause X-linked complete congenital stationary night blindness. Nat Genet 2000; 26:319-23. [PMID: 11062471]
7. Pusch CM, Zeitz C, Brandau O, Pesch K, Achatz H, Feil S, Scharfe C, Maurer J, Jacobi FK, Pinckers A, Andreasson S, Hardcastle A, Wissinger B, Berger W, Meindl A. The complete form of X-linked congenital stationary night blindness is caused by mutations in a gene encoding a leucine-rich repeat protein. Nat Genet 2000; 26:324-7. [PMID: 11062472]
8. Dryja TP, McGee TL, Berson EL, Fishman GA, Sandberg MA, Alexander KR, Derlacki DJ, Rajagopalan AS. Night blindness and abnormal cone electroretinogram ON responses in patients with mutations in the GRM6 gene encoding mGluR6. Proc Natl Acad Sci USA 2005; 102:4884-9. [PMID: 15781871]
9. Zeitz C, van Genderen M, Neidhardt J, Luhmann UF, Hoeben F, Forster U, Wycisk K, Mátyás G, Hoyng CB, Riemslag F, Meire F, Cremers FP, Berger W. Mutations in GRM6 cause autosomal recessive congenital stationary night blindness with a distinctive scotopic 15-Hz flicker electroretinogram. Invest Ophthalmol Vis Sci 2005; 46:4328-35. [PMID: 16249515]
10. Zeitz C, Forster U, Neidhardt J, Feil S, Kälin S, Leifert D, Flor PJ, Berger W. Night blindness-associated mutations in the ligand-binding, cysteine-rich, and intracellular domains of the metabotropic glutamate receptor 6 abolish protein trafficking. Hum Mutat 2007; 28:771-80. [PMID: 17405131]
11. Koike C, Obara T, Uriu Y, Numata T, Sanuki R, Miyata K, Koyasu T, Ueno S, Funabiki K, Tani A, Ueda H, Kondo M, Mori Y, Tachibana M, Furukawa T. TRPM1 is a component of the retinal ON bipolar cell transduction channel in the mGluR6 cascade. Proc Natl Acad Sci USA 2010; 107:332-7. [PMID: 19966281]
12. Duncan LM, Deeds J, Hunter J, Shao J, Holmgren LM, Woolf EA, Tepper RI, Shyjan AW. Down-regulation of the novel gene melastatin correlates with potential for melanoma metastasis. Cancer Res 1998; 58:1515-20. [PMID: 9537257]
13. Deeds J, Cronin F, Duncan LM. Patterns of melastatin mRNA expression in melanocytic tumors. Hum Pathol 2000; 31:1346-56. [PMID: 11112208]
14. Duncan LM, Deeds J, Cronin FE, Donovan M, Sober AJ, Kauffman M, McCarthy JJ. Melastatin expression and prognosis in cutaneous malignant melanoma. J Clin Oncol 2001; 19:568-76. [PMID: 11208852]
15. Fang D, Setaluri V. Expression and Up-regulation of alternatively spliced transcripts of melastatin, a melanoma metastasis-related gene, in human melanoma cells. Biochem Biophys Res Commun 2000; 279:53-61. [PMID: 11112417]
16. Miller AJ, Du J, Rowan S, Hershey CL, Widlund HR, Fisher DE. Transcriptional regulation of the melanoma prognostic

marker melastatin (TRPM1) by MITF in melanocytes and melanoma. Cancer Res 2004; 64:509-16. [PMID: 14744763]

17. Kim DS, Ross SE, Trimarchi JM, Aach J, Greenberg ME, Cepko CL. Identification of molecular markers of bipolar cells in the murine retina. J Comp Neurol 2008; 507:1795-810. [PMID: 18260140]
18. Koike C, Sanuki R, Miyata K, Koyasu T, Miyoshi T, Sawai H, Kondo M, Usukura J, Furukawa T. The functional analysis of TRPM1 in retinal bipolar cells. 30th Annual meeting Japan Neuroscience Society 2007; 58(Supplement 1):S41.
19. Morgans CW, Zhang J, Jeffrey BG, Nelson SM, Burke NS, Duvoisin RM, Brown RL. TRPM1 is required for the depolarizing light response in retinal ON-bipolar cells. Proc Natl Acad Sci USA 2009; 106:19174-8. [PMID: 19861548]
20. Audo I, Kohl S, Leroy BP, Munier FL, Guillonneau X, Mohand-Saïd S, Bujakowska K, Nandrot EF, Lorenz B, Preising M, Kellner U, Renner AB, Bernd A, Antonio A, Moskova-Doumanova V, Lancelot ME, Poloschek CM, Drumare I, Defoort-Dhellemmes S, Wissinger B, Léveillard T, Hamel CP, Schorderet DF, De Baere E, Berger W, Jacobson SG, Zrenner E, Sahel JA, Bhattacharya SS, Zeitz C. TRPM1 is mutated in patients with autosomal-recessive complete congenital stationary night blindness. Am J Hum Genet 2009; 85:720-9. [PMID: 19896113]
21. van Genderen MM, Bijveld MM, Claassen YB, Florijn RJ, Pearring JN, Meire FM, McCall MA, Riemslag FC, Gregg RG, Bergen AA, Kamermans M. Mutations in TRPM1 are a common cause of complete congenital stationary night blindness. Am J Hum Genet 2009; 85:730-6. [PMID: 19896109]
22. Li Z, Sergouniotis PI, Michaelides M, Mackay DS, Wright GA, Devery S, Moore AT, Holder GE, Robson AG, Webster AR. Recessive mutations of the gene TRPM1 abrogate ON bipolar cell function and cause complete congenital stationary night blindness in humans. Am J Hum Genet 2009; 85:711-9. [PMID: 19878917]
23. Onishi A, Peng GH, Hsu C, Alexis U, Chen S, Blackshaw S. Pias3-dependent SUMOylation directs rod photoreceptor development. Neuron 2009; 61:234-46. [PMID: 19186166]
24. Ueda Y, Iwakabe H, Masu M, Suzuki M, Nakanishi S. The mGluR6 5′ Upstream Transgene Sequence Directs a Cell-Specific and Developmentally Regulated Expression in Retinal Rod and ON-Type Cone Bipolar Cells. J Neurosci 1997; 17:3014-23. [PMID: 9096137]
25. Nakamura M, Ito S, Terasaki H, Miyake Y. Novel CACNA1F Mutations in Japanese Patients with Incomplete Congenital Stationary Night Blindness. Invest Ophthalmol Vis Sci 2001; 42:1610-6. [PMID: 11381068]
26. Chen S, Kadomatsu K, Kondo M, Toyama Y, Toshimori K, Ueno S, Miyake Y, Muramatsu T. Effects of flanking genes on the phenotypes of mice deficient in basigin/CD147. Biochem Biophys Res Commun 2004; 324:147-53. [PMID: 15464995]
27. Chang YF, Imam JS, Wilkinson MF. The nonsense-mediated decay RNA surveillance pathway. Annu Rev Biochem 2007; 76:51-74. [PMID: 17352659]
28. Yang K, Fang K, Fromondi L, Chan KW. Low temperature completely rescues the function of two misfolded K ATP channel disease-mutants. FEBS Lett 2005; 579:4113-8. [PMID: 16023110]
29. Smit LS, Strong TV, Wilkinson DJ, Macek M Jr, Mansoura MK, Wood DL, Cole JL, Cutting GR, Cohn JA, Dawson DC, Collins FS. Missense mutation (G480C) in the CFTR gene associated with protein mislocalization but normal chloride channel activity. Hum Mol Genet 1995; 4:269-73. [PMID: 7757078]
30. Ruan Y, Liu N, Priori SG. Sodium channel mutations and arrhythmias. Nat Rev Cardiol 2009; 6:337-48. [PMID: 19377496]
31. Mukerji N, Damodaran TV, Winn MP. TRPC6 and FSGS: the latest TRP channelopathy. Biochim Biophys Acta 2007; 1772:859-68. [PMID: 17459670]
32. Montell C. TRP channels in Drosophila photoreceptor cells. J Physiol 2005; 567:45-51. [PMID: 15961416]
33. Shen Y, Heimel JA, Kamermans M, Peachey NS, Gregg RG, Nawy S. A transient receptor potential-like channel mediates synaptic transmission in rod bipolar cells. J Neurosci 2009; 29:6088-93. [PMID: 19439586]
34. Werblin FS, Dowling JE. Organization of the retina of the mudpuppy, Necturus maculosus. II. Intracellular recording. J Neurophysiol 1969; 32:339-55. [PMID: 4306897]
35. Ayoub GS, Copenhagen DR. Application of a fluorometric method to measure glutamate release from single retinal photoreceptors. J Neurosci Methods 1991; 37:7-14. [PMID: 1677056]
36. Masu M, Iwakabe H, Tagawa Y, Miyoshi T, Yamashita M, Fukuda Y, Sasaki H, Hiroi K, Nakamura Y, Shigemoto R, Takada M, Nakamura K, Nakao K, Katsuki M, Nakanishi S. Specific deficit of the ON response in visual transmission by targeted disruption of the mGluR6 gene. Cell 1995; 80:757-65. [PMID: 7889569]
37. Nawy S. The metabotropic receptor mGluR6 may signal through G(o), but not phosphodiesterase, in retinal bipolar cells. J Neurosci 1999; 19:2938-44. [PMID: 10191311]
38. Dhingra A, Lyubarsky A, Jiang M, Pugh EN Jr, Birnbaumer L, Sterling P, Vardi N. The light response of ON bipolar neurons requires G[alpha]o. J Neurosci 2000; 20:9053-8. [PMID: 11124982]
39. Wang T, Jiao Y, Montell C. Dissecting independent channel and scaffolding roles of the Drosophila transient receptor potential channel. J Cell Biol 2005; 171:685-94. [PMID: 16301334]
40. Nishida M, Hara Y, Yoshida T, Inoue R, Mori Y. TRP channels: molecular diversity and physiological function. Microcirculation 2006; 13:535-50. [PMID: 16990213]
41. Westall CA, Dhaliwal HS, Panton CM, Sigesmun D, Levin AV, Nischal KK, Héon E. Values of electroretinogram responses according to axial length. Doc Ophthalmol 2001; 102:115-30. [PMID: 11518455]
42. Scholl HP, Langrova H, Pusch CM, Wissinger B, Zrenner E, Apfelstedt-Sylla E. Slow and fast rod ERG pathways in patients with X-linked complete stationary night blindness carrying mutations in the NYX gene. Invest Ophthalmol Vis Sci 2001; 42:2728-36. [PMID: 11581222]
43. Nakamura M, Lin K, Ito S, Terasaki H, Miyake Y. Novel NYX Mutations and Clinical Phenotype in Japanese Patients with Complete Congenital Stationary Night Blindness. ARVO Annual Meeting; 2003 May 4–9; Fort Lauderdale (FL).

44. Nakamura M, Miyake Y. Molecular genetic study of congenital stationary night blindness. Nippon Ganka Gakkai Zasshi 2004; 108:665-73. [PMID: 15584351]

The print version of this article was created on 9 March 2010. This reflects all typographical corrections and errata to the article through that date. Details of any changes may be found in the online version of the article.

TRPM1 is a component of the retinal ON bipolar cell transduction channel in the mGluR6 cascade

Chieko Koike[a], Takehisa Obara[b], Yoshitsugu Uriu[c], Tomohiro Numata[c], Rikako Sanuki[a], Kentarou Miyata[d], Toshiyuki Koyasu[d], Shinji Ueno[d], Kazuo Funabiki[e], Akiko Tani[a], Hiroshi Ueda[f], Mineo Kondo[d], Yasuo Mori[c], Masao Tachibana[b], and Takahisa Furukawa[a,1]

Departments of [a]Developmental Biology and [e]Systems Biology, Osaka Bioscience Institute, Osaka 565-0874, Japan; [b]Department of Psychology, Graduate School of Humanities and Sociology, University of Tokyo, Tokyo 113-0033, Japan; [c]Department of Synthetic Chemistry and Biological Chemistry, Graduate School of Engineering, Kyoto University, Kyoto 615-8510, Japan; [d]Department of Ophthalmology, Nagoya University Graduate School of Medicine, Nagoya 466-8550, Japan; and [f]Department of Biomolecular Science, Faculty of Engineering, Gifu University, Gifu 501-1193, Japan

Communicated by Constance L. Cepko, Harvard Medical School and Howard Hughes Medical Institute, Boston, MA, November 6, 2009 (received for review September 28, 2009)

An essential step in intricate visual processing is the segregation of visual signals into ON and OFF pathways by retinal bipolar cells (BCs). Glutamate released from photoreceptors modulates the photoresponse of ON BCs via metabotropic glutamate receptor 6 (mGluR6) and G protein (Go) that regulates a cation channel. However, the cation channel has not yet been unequivocally identified. Here, we report a mouse TRPM1 long form (TRPM1-L) as the cation channel. We found that TRPM1-L localization is developmentally restricted to the dendritic tips of ON BCs in colocalization with mGluR6. TRPM1 null mutant mice completely lose the photoresponse of ON BCs but not that of OFF BCs. In the TRPM1-L-expressing cells, TRPM1-L functions as a constitutively active nonselective cation channel and its activity is negatively regulated by Go in the mGluR6 cascade. These results demonstrate that TRPM1-L is a component of the ON BC transduction channel downstream of mGluR6 in ON BCs.

G protein | retina | photoresponse | glutamate | vision

Segregation of visual signals into ON and OFF pathways originates in BCs, the second-order neurons in the retina (1, 2). ON and OFF BCs express metabotropic glutamate receptors, mGluR6, and ionotropic glutamate receptors (iGluRs), respectively, on their dendrites (3–5). Reduction of glutamate released from photoreceptors by light stimulation depolarizes ON BCs and hyperpolarizes OFF BCs (6–8) mediated through respective glutamate receptors. The mGluR6 couples to a heterotrimeric G protein complex, Go (9, 10). Signals require Goα, which ultimately closes a downstream nonselective cation channel in ON BCs (6, 9, 11–13). However, this transduction cation channel in ON BCs has not been identified, despite intensive investigation.

In our screen to identify functionally important molecules in the retina, we found that *TRPM1* is predominantly expressed in retinal BCs. Most members of the TRP superfamily, which are found in a variety of sense organs, are non-voltage-gated cation channels (14–16). The founding member of the TRP family was discovered as a key component of the light response in *Drosophila* photoreceptors (17). *TRPM1*, also known as *melastatin*, was the first member of the melanoma-related transient receptor potential (TRPM) subfamily to be discovered (18, 19). *TRPM1* is alternatively spliced, resulting in the production of a long form (TRPM1-L) and a short N-terminal form devoid of transmembrane segments (TRPM1-S) (18, 20). Although mouse *TRPM1-S* was previously identified as *melastatin*, mouse *TRPM1-L* has not been identified (18). The distinct physiological and biological functions of TRPM1 still remain elusive, although some recent evidences including us suggested that TRPM1 might contribute to retinal BC function (21–23). Here, we show that TRPM1-L is the transduction cation channel of retinal ON BCs in the downstream of mGluR6 cascade.

Results

Isolation of Mouse *TRPM1-L*. We identified a mouse *TRPM1-L* cDNA (Fig. 1*A*) that corresponds to the human *TRPM1* long form (20). The mouse *TRPM1-L* encodes a predicted 1,622-aa protein, containing six transmembrane domains, a pore region, and a TRP domain, as do other major TRP family members (Fig. 1*A*). Northern blot analysis revealed the presence of both *TRPM1-L* and *-S* transcripts in the retina; however, only the latter was detected in the skin (Fig. 1*B*). In situ hybridization (ISH) showed the presence of substantial *TRPM1-L* transcripts in the inner nuclear layer (INL) at postnatal stages (Fig. 1*C*). Faint *TRPM1-S* signals were detected in the INL at postnatal day 9 (P9) (Fig. 1*D*). Immunostaining with anti-Chx10 antibody, a pan-BC marker, showed that *TRPM1-L* signals were located in BCs in the adult retina (Fig. 1*E*).

Localization of TRPM1-L on Dendritic Tips of ON BCs. Next, we raised an antibody against TRPM1-L (Fig. S1) and examined the localization of TRPM1-L (Fig. 1 *F–K* and Fig. S1). At P14, TRPM1-L was found diffusely in BC somata (Fig. 1*F*). At 1 month after birth, TRPM1-L localized to the dendritic tips in the outer plexiform layer (OPL) (Fig. 1*G*, arrows and stars). This labeling was not observed in the TRPM1 null mutant ($TRPM1^{-/-}$) mice (Fig. 2*D* and Fig. S1 *B–E*). To identify the subtypes of BCs expressing TRPM1-L, we coimmunostained BCs with anti-TRPM1 antibody and several adult retinal BC markers (Fig. 1 *H–K* and Fig. S1 *B–E*). Punctated TRPM1-L signals were localized at the tips of Goα-expressing and mGluR6-expressing dendrites (Fig. 1 *H* and *I*, and Table S1). We also coimmunostained TRPM1-L with PNA that binds to glycoconjugates associated with the cell membrane and the intersynaptic matrix of cone terminals. The continuous punctated TRPM1-L signals appeared in register with the PNA signals, suggesting that TRPM1-L is localized adjacent to cone photoreceptors as well as to rod photoreceptors (Fig. 1*J*, indicated by stars, and Table S1). Actually, TRPM1-L was not expressed in photoreceptor terminals because the punctated TRPM1-L signals did not colocalize with bassoon, a marker for the presynaptic photoreceptor structures (Fig. 1*K* and Table S1). We did not observe distinct colocalization of TRPM1-L with OFF-BC markers (Fig. S2).

Author contributions: C.K. and T.F. designed research; C.K., T.O., Y.U., T.N., R.S., K.M., T.K., S.U., K.F., A.T., H.U., and T.F. performed research; M.K., Y.M., and M.T. contributed new reagents/analytic tools; C.K., T.O., Y.U., T.N., K.M., T.K., S.U., K.F., H.U., M.K., Y.M., M.T., and T.F. analyzed data; and C.K., M.K., Y.M., M.T., and T.F. wrote the paper.

The authors declare no conflict of interest.

Freely available online through the PNAS open access option.

Database deposition: The nucleotide sequence for the mouse TRPM1-L gene has been deposited in the GenBank database (accession no. AY180104).

[1]To whom correspondence should be addressed. E-mail: furukawa@obi.or.jp.

This article contains supporting information online at www.pnas.org/cgi/content/full/0912730107/DCSupplemental.

www.pnas.org/cgi/doi/10.1073/pnas.0912730107

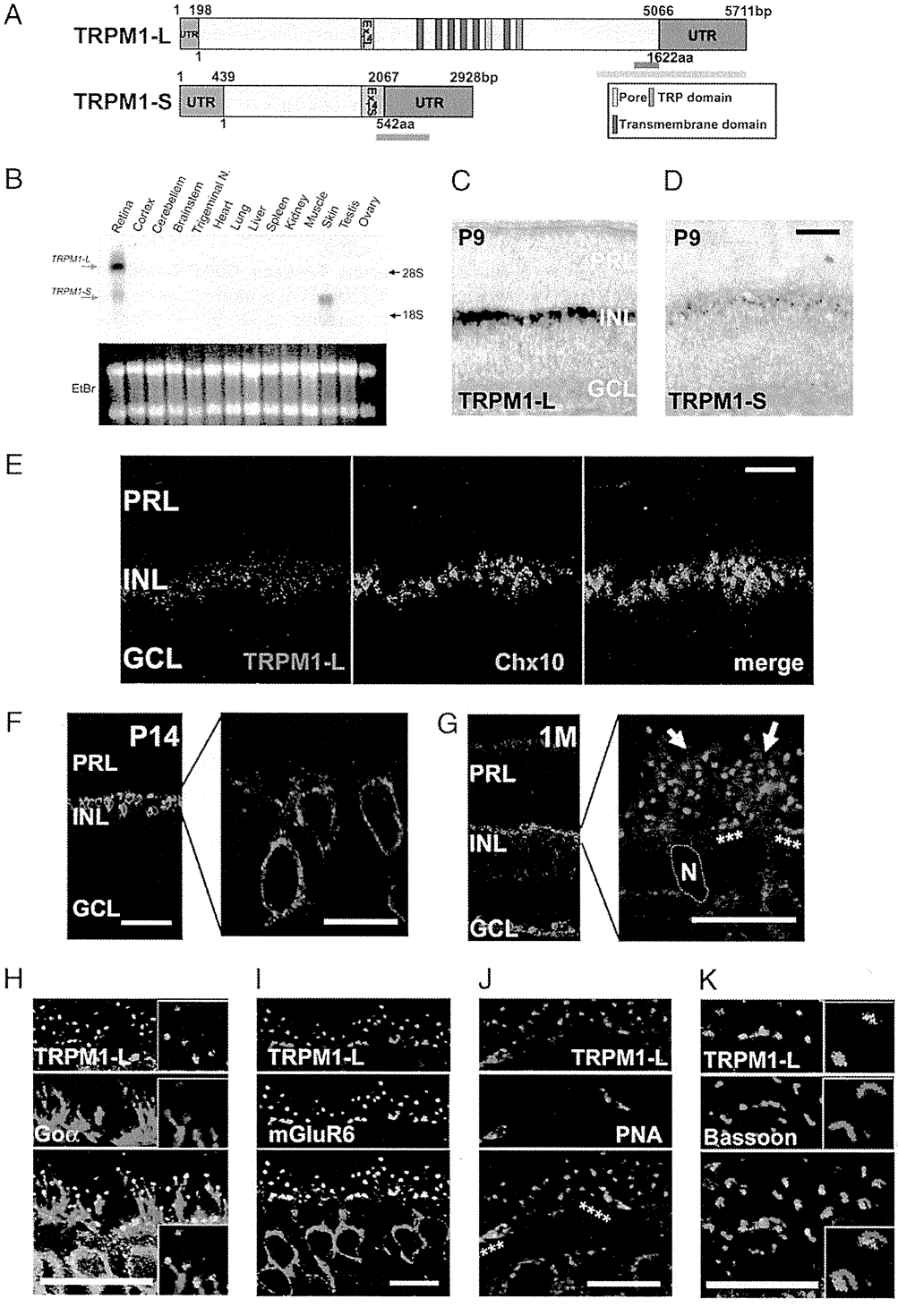

Fig. 1. The molecular analysis and expression of mouse *TRPM1-L*. (*A*) Schematic diagrams of full-length mouse TRPM1-L and TRPM1-S genes and their ORFs. Light gray boxes represent ORF, and light purple boxes indicate exon 14 (L and S). Green and pink bars indicate sequences used for *TRPM1-L*- or *TRPM1-S*-specific probes, respectively. The red bar indicates amino acid sequence used for generating anti-TRPM1-L antibody. (*B*) Northern blot analysis of mouse *TRPM1* transcription in adult mouse tissues. The sizes of *TRPM1-L* and *TRPM1-S* transcripts are ≈6 kb and 3 kb, respectively. Both *TRPM1-L* and *-S* transcripts were detected in the retina; however, only the *TRPM1-S* transcript was detected in the skin. (*Lower*) Ethidium bromide staining of RNA. Each lane contains ≈10 μg of total RNA. Trigeminal N., trigeminal nucleus. (*C* and *D*) ISH analysis of mouse *TRPM1* in the postnatal retina. *TRPM1-L*-specific signal was detected in the INL at P9 (*C*). *TRPM1-S* was detected in the INL at P9 (*D*). PRL, photoreceptor layer; INL, inner nuclear layer; GCL, ganglion cell layer. (Scale bar: 100 μm.) (*E*) ISH of *TRPM1-L* mRNA and following immunostaining of anti-Chx10 antibody, a pan-BC marker. (Scale bar: 50 μm.) (*F* and *G*) Immunostaining with an antibody against TRPM1-L exhibited TRPM1-L signals in cell bodies of retinal BCs at P14 (*F*) and at dendritic tips of retinal BCs (stars and arrows) at 1 M (*G*). N, nucleus of a BC. (Scale bars: 50 μm.) (*H–K*) Confocal images of OPLs double-labeled with anti-TRPM1-L antibody and other retinal markers. TRPM1-L-positive puncta were localized at the tips of Goα distribution (*H*). TRPM1-L-positive puncta were colocalized with mGluR6 staining (*I*). Continuous puncta marked with TRPM1-L were colocalized with PNA (stars) (*J*). TRPM1-L-positive puncta were surrounded by synaptic ribbons stained with bassoon (*K*). (Scale bars: 10 μm.)

TRPM1–L Is Required for the Photoresponse of ON BCs. To address a possible role of TRPM1 in ON BC function, we generated *TRPM1* null mutant (*TRPM1*$^{-/-}$) mice by targeted gene disruption (Fig. 2*A*). We used Southern blots to confirm the exons 4–6 deletion (Fig. 2*B*). Northern blot analysis showed that no substantial transcripts were detected in *TRPM1*$^{-/-}$ retinas (Fig. 2*C*). Although *TRPM1-S* is expressed in the skin, *TRPM1*$^{-/-}$ mice were indistinguishable from wild-type (WT) littermates in appearance, including coat color. In *TRPM1*$^{-/-}$ mice, immunoreactivity to TRPM1-L was essentially undetectable (Fig. 2*D*). In contrast, no substantial reduction of retinal BC markers including Chx10, Goα, and mGluR6 was observed in *TRPM1*$^{-/-}$ mouse retinas at 1 month (Fig. 2 *E–G*).

To examine whether TRPM1-L can function as a transduction cation channel in rod and cone ON BCs, we applied whole-cell recording techniques to BCs in mouse retinal slices (Fig. 3). Under the whole-cell voltage clamp, light stimulation induced an inward current in ON BCs of WT mice (Fig. 3*A*, WT), reflecting the opening of transduction cation channels via mGluR6 deactivation (11, 13, 24, 25). On the other hand, neither rod BCs nor cone ON BCs of *TRPM1*$^{-/-}$ mice evoked photoresponses (Fig. 3*A*, TRPM1 KO). Collected data showed significant differences

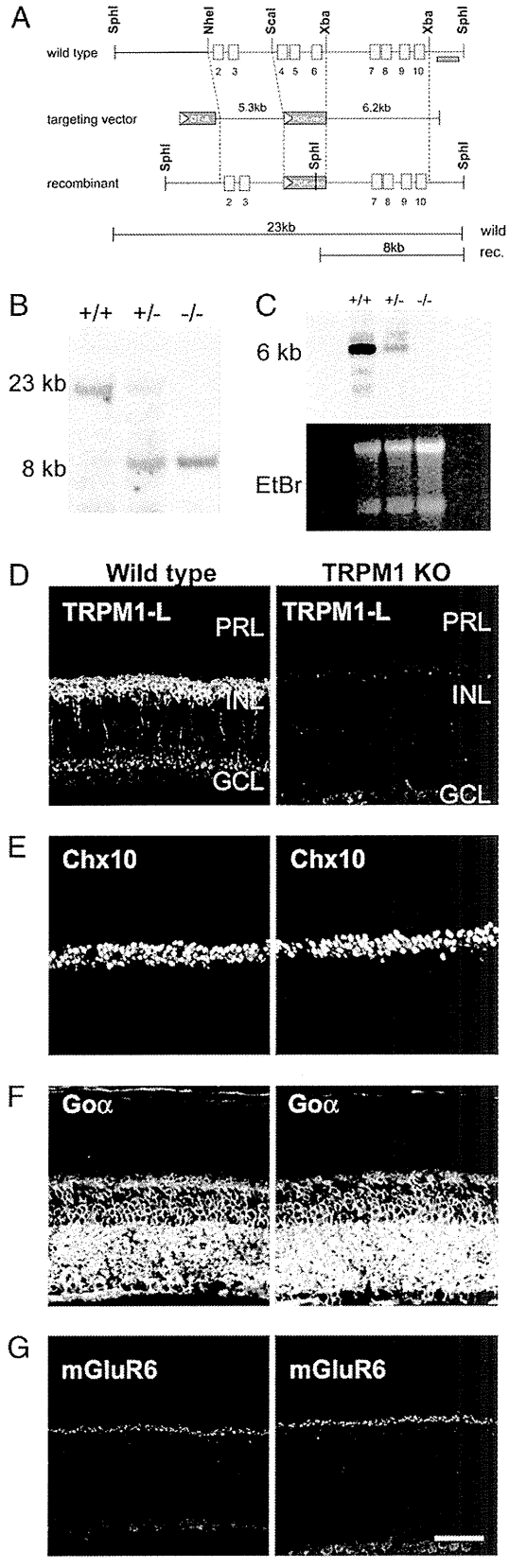

Fig. 2. Generation of *TRPM1*$^{-/-}$ mouse by targeted gene disruption. (*A*) Strategy for the targeted deletion of *TRPM1* gene. The open boxes indicate exons. Exons 4–6 were replaced with the *PGK-neo* cassette. The probe used for Southern blot analysis is shown as a dark bar. (*B*) Southern blot analysis of genomic DNA. *SphI*-digested genomic DNA was hybridized with a 3′ outside probe, detecting 23-kb WT and 8-kb mutant bands. (*C*) Northern blot analysis of total RNA extracted from the retina derived from WT, *TRPM1*$^{+/-}$, and *TRPM1*$^{-/-}$ mice using cDNA probe derived from exons 3–9. (*D–G*) Immunostaining of WT and *TRPM1*$^{-/-}$ retinal sections at 1 M. The TRPM1-L signal in the INL of WT mouse retina disappeared in the *TRPM1*$^{-/-}$ mouse retina (*D*). Immunohistochemical analysis using antibodies to Chx10 [pan-BC nuclei marker (*E*)], Goα [ON BC dendrite marker (*F*)], and mGluR6 [ON BC dendrite tip marker (*G*)] showed no obvious difference between WT and *TRPM1*$^{-/-}$ mice retinas. PRL, photoreceptor layer; INL, inner nuclear layer; GCL, ganglion cell layer. (Scale bar: 50 μm.)

in the amplitude of photoresponses between WT and *TRPM1*$^{-/-}$ mice (Fig. 3*B*). Membrane current fluctuations of ON BCs in the dark were much smaller in *TRPM1*$^{-/-}$ mice than in WT mice (Fig. 3*A*), suggesting that there are no functional transduction cation channels in ON BCs of *TRPM1*$^{-/-}$ mice (Fig. 3*C*). On the other hand, light stimulation of cone OFF BCs in both WT and *TRPM1*$^{-/-}$ mice evoked photoresponses (Fig. 3*D*). We detected no significant differences in either the amplitude of the light responses (Fig. 3*E*) or the time for half-maximal amplitude after the light was turned off ($T_{1/2}$) (Fig. 3*F*).

Functional Coupling Between TRPM1-L and mGluR6. To examine whether or not TRPM1-L is modulated by mGluR6 activation, we measured ionic currents in *TRPM1-L*-trasnfected CHO cells under whole-cell voltage clamp. We measured the amplitude of the inward current at −100 mV, which was plotted against time to examine the effects of glutamate and *N*-methyl-D-glucamine ($NMDG^+$), an impermeant cation. In the CHO cells expressing mGluR6, Goα, and TRPM1-L, constitutively active inward currents were observed, whereas in *Goα*-transfected CHO cells stably expressing mGluR6 but not TRPM1-L ($n = 11$), a whole-cell current was negligible (Fig. 4*A*). The *I–V* relationship of the inward currents was almost linear with a reversal potential (V_{rev}) of ~0 mV (0.92 mV, $n = 15$), indicating that, like most TRP channels, TRPM1-L may be a nonselective cation channel (Fig. 4*A*). In fact, replacement of extracellular cations with $NMDG^+$ resulted not only in the reduction of the current but also in a shift of V_{rev} toward hyperpolarizing potential ($\Delta V_{rev} = -23.7$ mV, $n = 15$) (Fig. 4*A*). Constitutively active currents were detected even by the replacement of extracellular cations with either Na^+, K^+, Ca^{2+}, or Mg^{2+}, supporting the idea that TRPM1-L is a constitutively active nonselective cation channel (26) (Fig. S3*A*). In CHO cells expressing mGluR6, Goα, and TRPM1-L, constitutively active cationic currents were suppressed by the addition of 1 mM glutamate to the bath solution (Fig. 4*A*). Although in CHO cells cotransfected with *Goα* and *TRPM1-L*, whole-cell currents with similar *I–V* relationships were detected, application of glutamate did not affect the whole-cell current (in 11 of 11 cells). A calculated average suppression ratio of inward current ($V_h = -100$ mV) by 1 mM glutamate administration was 52.7% ($n = 15$) in CHO cells expressing mGluR6, Goα, and TRPM1-L, whereas the average suppression ratio in CHO cells coexpressing Goα and TRPM1-L was 2.1% ($n = 11$) (Fig. 4*A*). The effects of glutamate were reversible (Fig. 4*A*).

We investigated the effect of Go activation on the TRPM1-L current by measuring a whole-cell current in TRPM1-expressing CHO cells transfected either with wild-type of *Goα (Goα)* or a constitutively active mutant of *Goα (Goα-Q205L)*. Analysis of the reduced currents upon replacement of extracellular Na^+ with $NMDG^+$ demonstrated that the current density obtained in *TRPM1-L*-transfected cells (3.53 pA/pF, $n = 8$) was considerably larger than that in vector-transfected control cells (0.50 pA/pF, $n = 6$) and that in *TRPM-L-* and *Goα*-cotransfected cells (1.89 pA/pF, $n = 14$) (Fig. 4*B*). Furthermore, intracellular application of GMP-PNP (1 mM), an unhydrolyzable analog of GTP, to

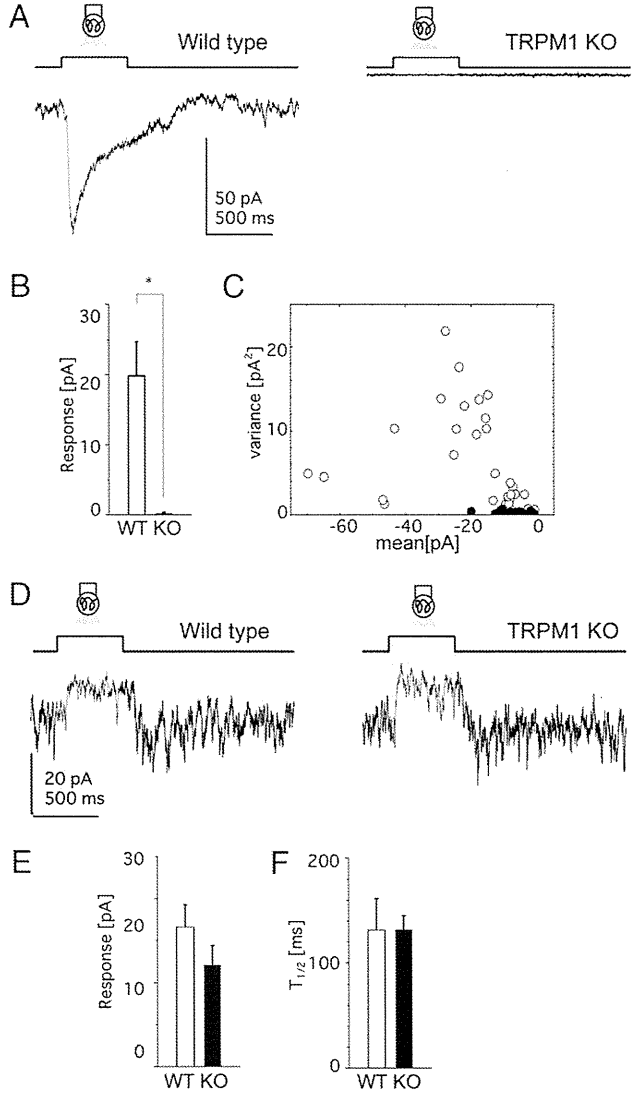

Fig. 3. TRPM1-L is essential for ON BC photoresponses. (*A–C*) Data from ON BCs in the retinal slice preparation. (*A*) Photoresponses of ON BCs from WT (*Left*) and *TRPM1*$^{-/-}$ (*Right*) mice (holding potential at −62 mV). Each trace illustrates the average of three responses. (*B*) Mean ± SEM of photoresponses from WT (15 cells, 12 mice) and *TRPM1*$^{-/-}$ (9 cells, 8 mice) mice. *, $P < 0.05$. (*C*) The variance against the mean (the leak current not subtracted) of the dark membrane current fluctuations obtained from WT (open circles: 34 traces, 15 cells) and *TRPM1*$^{-/-}$ (filled circles: 26 traces, 9 cells) mice. (*D–F*) Data from OFF BCs in the retinal slice preparation. (*D*) Photoresponses of OFF BCs from WT (*Left*) and *TRPM1*$^{-/-}$ (*Right*) mice under similar recording conditions as in *A*. Each trace illustrates the average of two responses. No significant difference in the response amplitude (WT, 5 cells; *TRPM1*$^{-/-}$, 6 cells) (*E*) or in the time for half-maximal amplitude after the termination of light stimulation ($T_{1/2}$) (WT, 5 cells; *TRPM1*$^{-/-}$, 6 cells) (*F*).

TRPM1-L- and *Goα*-cotransfected cells resulted in a remarkable decrease of current density (1.00 pA/pF, $n = 22$), whereas intracellular application of GDPβS (1 mM), an unhydrolyzable analog of GDP, restored the current density to a level comparable to that in *TRPM1-L*-transfected cells (3.35 pA/pF, $n = 9$) (Fig. 4*B*). We also observed suppression of current density in *TRPM1-L*- and *Goα-Q205L*-cotransfected cells to a level comparable to that in *TRPM1-L*- and *Goα*-cotransfected cells intracellularly perfused with GMP-PNP (1.00 pA/pF, $n = 36$) (Fig. 4*B*). We confirmed that the expression level of TRPM1-L protein was not significantly affected by Goα expression with a pull-down assay of biotinylated membrane proteins (Fig. S3*B*). These results suggest that TRPM1-L channel function is negatively regulated by Go activation.

To confirm that TRPM1-L channel activity is regulated via Go proteins in the mGluR6 signal cascade, we performed single-channel recordings in the outside-out patch mode (Fig. 4*C*). In mGluR6-stably expressed CHO cells transfected with both *TRPM1-L* and *Goα*, constitutively active currents, whose single-channel conductance was 76.70 pS and open probability (NP_O) was 0.48, were obtained in 41 cells out of 129 cells. These currents showed a V_{rev} of ~0 mV (6.86 mV, $n = 21$). By contrast, similar single-channel currents were absent in cells expressing both mGluR6 and Goα but not TRPM1-L ($n = 32$) (Fig. S3*C*). We next examined whether these single-channel currents were regulated by the mGluR6 signal cascade. Analyses of time-dependent changes in *NPo* demonstrated a reversible suppression of *NPo* by 1 mM glutamate application (in 7 of 16 cells) (Fig. 4*C*). The average *NPo* suppression ratio was 65.0% ($n = 7$). The average amplitude of single-channel currents in *TRPM1-L*-transfected cells was −4.60 pA ($n = 30$), and that in 2 mM Ca^{2+}- and 1 mM Mg^{2+}-containing solution was significantly reduced to −1.01 pA ($n = 10$) (Fig. 4*D*).

To demonstrate more directly that TRPM1-L is regulated by Go protein, the effect of addition of the purified Go protein from the intracellular side on TRPM1-L activity was tested in the excised inside-out patch mode (Fig. 4*E*). We confirmed that the purified Go protein contains mainly Goα by Western blotting and silver staining (27, 28). In *TRPM1-L*-transfected cells, we detected similar single-channel currents (−4.60 pA, $n = 43$) as observed in Fig. 4*C*. Application of the purified Go protein gradually but strongly suppressed *NPo* (by 80.2%, in 16 of 16 cells) within 60 s, whereas administration of heat-denatured Go protein failed to suppress *NPo* (by 0.6%, in 14 of 14 cells) with GMP-PNP (Fig. 4*E*).

Discussion

Recently, it was suggested that TRP channels have a possible function in retinal BCs (22, 23). Bellone et al. (22) reported that *TRPM1* may be responsible for horse congenital stationary night blindness (CSNB), from their observation that *TRPM1* expression was decreased in CSNB (*LP/LP*) Appaloosa horses among five genes within the *LP* candidate region of the equine genome. Although mutations of TRPM1 in *LP/LP* horse were not identified, they even speculated that *TRPM1* might be a transduction cation channel in retinal ON BCs. Shen et al. (23) investigated whether or not TRPV1 is a retinal ON BC transduction channel. ON BCs responded to TRPV1 agonists; however, photoresponses of ON BCs in *TRPV1*$^{-/-}$ mice were normal. Based on the absence of the dark-adapted ERG b-wave in the *Trpm1*^{tm1Lex} mutant mouse, they speculated that ON BC function would be disrupted in these mice (23). We also examined the optokinetic responses (OKRs) and electroretinograms (ERGs) of 2-month-old WT and *TRPM1*$^{-/-}$ mice. Optokinetic deficiencies similar to those of mice lacking mGluR6 (29) were observed in *TRPM1*$^{-/-}$ mice. It is interesting that the OFF pathway did not compensate for the loss of the ON pathway in spatial processing. In contrast to this result, patients lacking mGluR6 receptors were behaviorally normal, suggesting some OFF pathway redundancy and/or compensation (30). The ERG b-wave, originating mainly from the rod BCs, in *TRPM1*$^{-/-}$ mice was not present. In the light-adapted state, the ERG b-wave was severely depressed or absent leaving only the ERG a-wave in the *TRPM1*$^{-/-}$ mouse (21). These ERG results suggested that both the function of rod and cone BCs, and the signal transmission from rod and cone photoreceptors to BCs were severely impaired in *TRPM1*$^{-/-}$ mice.

In this study, we show that TRPM1-L is essential for the light-evoked response of ON BCs and that TRPM1-L meets the criteria for the transduction cation channel as follows. (*i*) Immunohistochemical experiments revealed that TRPM1-L is specifically expressed in ON BCs, especially at the dendritic tips in colocalization with mGluR6.

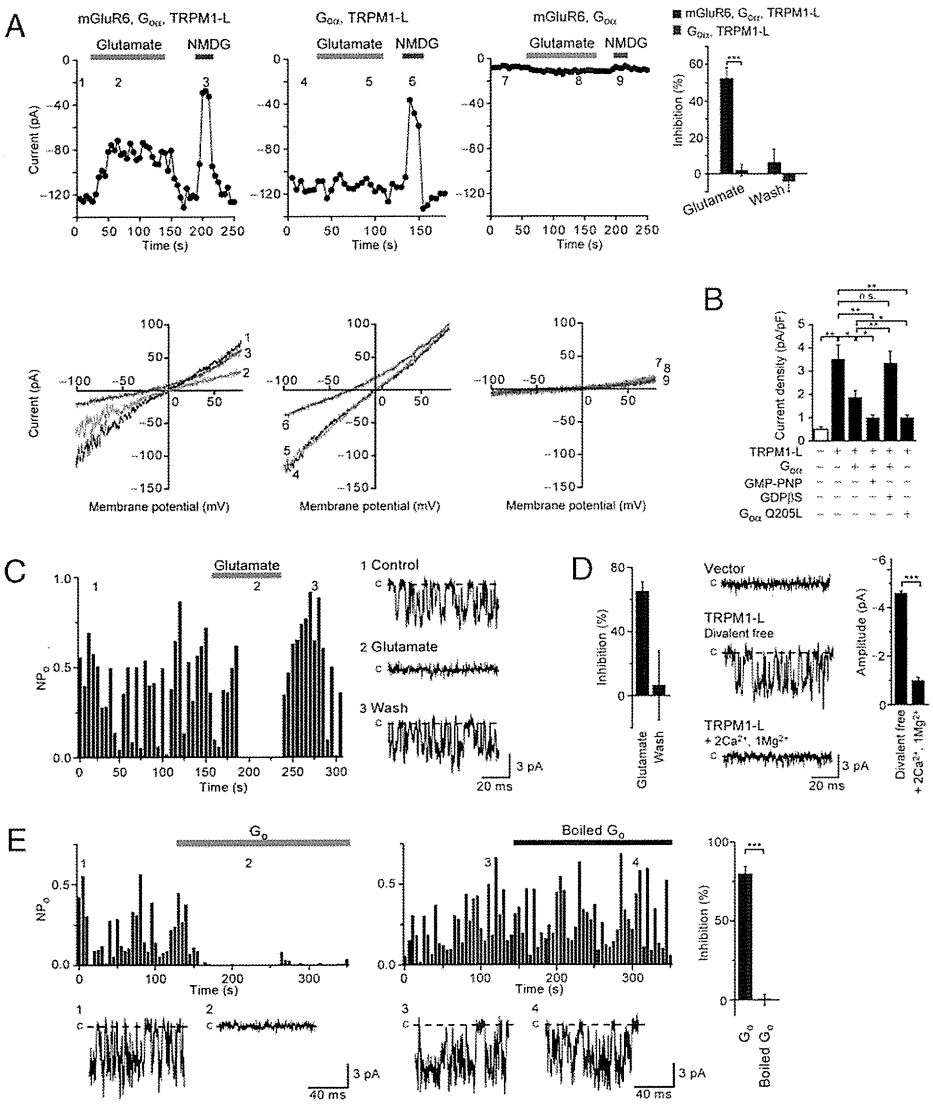

Fig. 4. Functional coupling of TRPM1-L with mGluR6 is mediated by Go protein in CHO cells. (*A*) mGluR6 activation inhibits cationic currents by TRPM1-L in CHO cells. Effects of 1 mM glutamate and replacement of extracellular Na^+ with $NMDG^+$ on whole-cell currents recorded in cells expressing different combinations of constructs as indicated above each plot at –100 mV (*Upper*) in the 180-ms voltage ramp (applied every 5 s) from +80 mV to –100 mV (V_h = –60 mV) before (1, 4, 7) and during (2, 5, 8) glutamate application and replacement of extracellular Na^+ with $NMDG^+$ (3, 6, 9) (*Lower*). The bar graphs represent suppression ratios of currents at ≈100 mV during and after activation of mGluR6 in CHO cells expressing mGluR6, Goα, and TRPM1-L (n = 15) or Goα and TRPM1-L (n = 11). (*B*) Inhibitory effects of Goα constructs on Na^+ currents via TRPM1-L (–60 mV). (*C*) Suppression of single TRPM1-L channel activity (NP_O) at –60 mV by activation of mGluR6 in excised outside-out patches. The bar graph shows the averaged NP_O suppression ratio (n = 10). (*D*) Extracellular divalent cations reduce the single-channel current amplitude of TRPM1-L in outside-out patches. The bar graph at the right represents average single TRPM1-L channel amplitudes in divalent cation-free (n = 29) or Ca^{2+}- and Mg^{2+}-containing (n = 11) solution. (*E*) Inhibition of NP_O of TRPM1-L by intracellular treatment of Go protein in inside-out patches. The bar graphs show averaged NP_O suppression ratio by intracellular application of activated (n = 16) and boiled (n = 14) Go protein. Data represent the mean ± SEM. n.s., not significant. *, $P < 0.05$; **, $P < 0.01$; ***, $P < 0.001$.

(*ii*) Retinal slice patch recordings from the *TRPM1*$^{-/-}$ mice show that photoresponses disappear in ON BCs but remain intact in OFF BCs. Other cellular properties of the ON BCs were unaffected in the *TRPM1*$^{-/-}$ mice (e.g., leak and calcium currents), suggesting that compensatory changes or general cellular malfunction did not occur in *TRPM1*$^{-/-}$ mice. (*iii*) Application of patch-clamp techniques to the TRPM1-expressing cells found that TRPM1-L is a nonselective cation channel and that the TRPM1-L activity is negatively regulated by the glutamate-activated mGluR6–Goα signaling cascade. Thus, we clearly demonstrate that TRPM1-L is a component of the transduction cation channel in the mGluR6 cascade of retinal ON BCs.

Materials and Methods

Molecular Cloning and Construction of Mouse *TRPM1-L* Expression Vector. We screened the UniGene databases by Digital Differential Display (DDD) and found UniGene Cluster Mm.58616, which contains ESTs (expressed sequence tags) enriched in the eye and the skin. Represented EST sequences encoded *TRPM1-S* (*melastatin*, *trpm1 short form*). We screened a mouse P0-P3 retinal cDNA library using a 1,703-bp fragment of the mouse *melastatin* cDNA (283-1991 bp of #AF047714) and isolated the mouse TRPM1 long form (*TRPM1-L*). *TRPM1-L* cDNA was subcloned into a modified *pCAGGS* vector (31).

Immunohistochemistry. Mouse eye cups were fixed, cryoprotected, embedded, frozen, and sectioned 20 μm thick. For immunostaining, we used the following primary antibodies: anti-Goα antibody (mouse monoclonal, Chemicon, #MAB3073), anti-bassoon antibody (mouse monoclonal, Stressgen, #VAM-PS003), and anti-Chx10 antibody [rabbit polyclonal, our production (32)].

Antibody Production. A cDNA encoding a C-terminal portion of mouse TRPM1-L (residues 1554–1622 aa, TRPM1-L-C) was subcloned into *pGEX4T-1* (Amersham). We confirmed, either by immunohistochemistry or Western blotting, that the signals detected by this antibody in the retina disappeared in *TRPM1*$^{-/-}$ mice (Fig. S1). The antibody against mGluR6 was raised in Guinea Pigs with synthetic peptides [KKTSTMAAPPKSENSEDAK] (853-871, GenBank #NP_775548.2). We confirmed that the signals detected by this antibody in the retina disappeared in *mGluR6*$^{-/-}$ mice and by preincubation with 5.7 μg/mL synthetic peptides as molar ratio 1:100 with antibody.

Generation of *TRPM1*-Null Mutant Mice. We deleted exons 4–6 of the TRPM1 gene to produce the targeting construct for the targeted gene disruption of TRPM1. The linearized targeting construct was transfected into TC1 embryonic stem cell line (33).

Retinal Slice Preparation and Recordings. Adult (postnatal day <28) *129Sv/Ev* (WT) mice were dark adapted for ≈20 min, and retinal slices were prepared as described in ref. 34. At the end of perforated patch recordings, the patch membrane was ruptured to introduce Lucifer yellow from the patch pipette into the cell and then its morphology was examined by epifluorescence microscopy (35–37). The extracellular solution contained 120 mM NaCl, 3.1 mM KCl, 2 mM $CaCl_2$, 1 mM $MgSO_4$, 23 mM $NaHCO_3$, 0.5 mM KH_2PO_4, and 6 mM D-glucose (pH adjusted to 7.6 with 95% O_2/5% CO_2 at 36°C). The

pipette solution for recordings consisted of 105 mM $CsCH_3SO_3$, 0.5 mM $CaCl_2$, 5 mM EGTA, 20 mM Hepes, 10 mM TEA-Cl, 5.5 mM $MgCl_2$, 5 mM ATP disodium salt, 0.5 mM GTP disodium salt, and 0.25% Lucifer yellow dipotassium salt (pH adjusted to 7.6 with CsOH). For perforated patch recordings, 0.5 mg/mL amphotericin B (Sigma) was added to the pipette solution. The retinal slice was diffusely illuminated (2.3×10^4 photons·μm^{-2}·s^{-1}) by a light-emitting diode (emission maximum at 520 nm) from underneath the recording chamber.

Recombinant Expression and Current Recording in CHO Cells. Whole-cell and patch recordings were performed on CHO cells at room temperature (22-25°C) with an EPC-9 (Heka Electronic) or Axopatch 200B (Axon Instruments) patch-clamp amplifier as described in ref. 24. For whole-cell recordings, the Na^+-based bath solution contained 145 mM NaCl, 10 mM Hepes, 10 mM D-glucose, and 10 mM D-mannitol (pH adjusted to 7.4 with NaOH). The pipette solution contained 145 mM CsCl, 2.86 mM $CaCl_2$, 1 mM $MgCl_2$, 5 mM EGTA, and 10 mM Hepes (pH adjusted to 7.4 with CsOH). The free Ca^{2+} concentration of this solution was calculated to be 200 nM as computed with Maxchelator (38). The suppression ratio (%) in Fig. 4*A* was calculated according to the following equation: suppression ratio (%) = $100 \times \{1 - (I_{Glu} - I_{NMDG})/(I_{Ctl} - I_{NMDG})\}$, where I_{Ctl} and I_{Glu} are whole-cell current observed before and during 1 mM glutamate application at −100 mV, respectively. I_{NMDG} represents the current observed during $NMDG^+$-replacement of extracellular cations with $NMDG^+$. Single-channel recordings were performed in the excised inside-out or outside-out configuration. Activity plots of open probability (NP_O; N is the number of channels in the patch and P_O is the single-channel open probability) recorded from inside-out and outside-out patches, as calculated for a series of 500-ms test pulses to −60 mV and plotted as a vertical bar on the activity histogram. The NP_O of single channels was calculated by dividing the total time spent in the open state by the total time of continuous recording (500 ms) in the patches containing active channels. The amplitude of single-channel currents was measured as the peak-to-peak distance in Gaussian fits of the amplitude histogram. For outside-out recordings, the extracellular side was exposed to a bath solution containing 140 mM KCl, 10 mM Hepes, 5 mM D-glucose, and 25 mM D-mannitol (pH adjusted to 7.4 with KOH). To observe the effects of extracellular divalent cations, 2 mM $CaCl_2$ and 1 mM $MgCl_2$ were added to bath solution. The pipette solution was composed of 145 mM CsCl, 2.86 mM $CaCl_2$, 1 mM $MgCl_2$, 5 mM EGTA, and 10 mM Hepes (pH adjusted to 7.4 with CsOH). The suppression ratio (%) in Fig. 4*C* was calculated according to the following equation: suppression ratio (%) = $100 \times \{1 - NP_{O\,Glu}/NP_{O\,Ctl}\}$, where $NP_{O\,Ctl}$ and $NP_{O\,Glu}$ indicate mean NP_O of six traces obtained before and during 1 mM glutamate application, respectively. For inside-out recordings, the intracellular side was exposed to a Cs^+-based bath solution consisting of 145 mM CsCl, 2.86 mM $CaCl_2$, 1 mM $MgCl_2$, 5 mM EGTA, and 10 mM Hepes (pH adjusted to 7.4 with CsOH), and an extracellular (pipette) solution that contained 140 mM KCl, 10 mM Hepes, 5 mM D-glucose, and 25 mM D-mannitol (pH adjusted to 7.4 with KOH) was used. Purified Go protein was activated by 100 nM GMP-PNP for 30 min at 4° C (Go) or denaturated by boiling for 10 min at 95°C (Boiled Go) before use. The suppression ratio (%) in Fig. 4*E* was calculated according to the following equation: suppression ratio (%) = $100 \times \{1 - NP_{O\,Go}/NP_{O\,Ctl}\}$, where $NP_{O\,Ctl}$ and $NP_{O\,Go}$ indicate mean NP_O of six traces obtained before and during activated or boiled Go protein application.

ACKNOWLEDGMENTS. We thank Drs. M. Okazawa, N. Wada, T. Doi, M. Wakamori, S. Kiyonaka, N. Kajimura, and J. Usukura for technical advice and M. Kadowaki, H. Tsujii, Y. Kawakami, M. Joukan, K. Sone, and S. Kennedy for technical assistance. This work was supported by a Grant for Molecular Brain Science (to T.F.), Grants-in-Aid for Scientific Research (B) (to T.F.) and (C) (to C.K.) from the Ministry of Education, Culture, Sports, Science and Technology of Japan, PREST program from Japan Science and Technology Agency (to C.K.), and grants from the Takeda Science Foundation, the Uehara Memorial Foundation, and the Mochida Memorial Foundation (to T.F.).

1. Dowling JE (1987) *The Retina: An Approachable Part of the Brain* (Belknap Press of Harvard Univ Press, Cambridge, MA).
2. DeVries SH, Baylor DA (1993) Synaptic circuitry of the retina and olfactory bulb. *Cell* 72 (Suppl):139–149.
3. Nomura A, et al. (1994) Developmentally regulated postsynaptic localization of a metabotropic glutamate receptor in rat rod bipolar cells. *Cell* 77:361–369.
4. Haverkamp S, Grünert U, Wässle H (2001) Localization of kainate receptors at the cone pedicles of the primate retina. *J Comp Neurol* 436:471–486.
5. Morigiwa K, Vardi N (1999) Differential expression of ionotropic glutamate receptor subunits in the outer retina. *J Comp Neurol* 405:173–184.
6. de la Villa P, Kurahashi T, Kaneko A (1995) L-glutamate-induced responses and cGMP-activated channels in three subtypes of retinal bipolar cells dissociated from the cat. *J Neurosci* 15:3571–3582.
7. Masu M, et al. (1995) Specific deficit of the ON response in visual transmission by targeted disruption of the mGluR6 gene. *Cell* 80:757–765.
8. Euler T, Schneider H, Wässle H (1996) Glutamate responses of bipolar cells in a slice preparation of the rat retina. *J Neurosci* 16:2934–2944.
9. Weng K, et al. (1997) Functional coupling of a human retinal metabotropic glutamate receptor (hmGluR6) to bovine rod transducin and rat Go in an in vitro reconstitution system. *J Biol Chem* 272:33100–33104.
10. Vardi N (1998) Alpha subunit of Go localizes in the dendritic tips of ON bipolar cells. *J Comp Neurol* 395:43–52.
11. Nawy S (1999) The metabotropic receptor mGluR6 may signal through G(o), but not phosphodiesterase, in retinal bipolar cells. *J Neurosci* 19:2938–2944.
12. Dhingra A, et al. (2002) Light response of retinal ON bipolar cells requires a specific splice variant of Galpha(o). *J Neurosci* 22:4878–4884.
13. Shiells RA, Falk G (1990) Glutamate receptors of rod bipolar cells are linked to a cyclic GMP cascade via a G-protein. *Proc Biol Sci* 242:91–94.
14. Ramsey IS, Delling M, Clapham DE (2006) An introduction to TRP channels. *Annu Rev Physiol* 68:619–647.
15. Clapham DE (2003) TRP channels as cellular sensors. *Nature* 426:517–524.
16. Owsianik G, Talavera K, Voets T, Nilius B (2006) Permeation and selectivity of TRP channels. *Annu Rev Physiol* 68:685–717.
17. Montell C (2001) Physiology, phylogeny, and functions of the TRP superfamily of cation channels. *Sci STKE* 2001:re1.
18. Duncan LM, et al. (1998) Down-regulation of the novel gene melastatin correlates with potential for melanoma metastasis. *Cancer Res* 58:1515–1520.
19. Kraft R, Harteneck C (2005) The mammalian melastatin-related transient receptor potential cation channels: an overview. *Pflugers Arch* 451:204–211.
20. Hunter JJ, et al. (1998) Chromosomal localization and genomic characterization of the mouse melastatin gene (Mlsn1). *Genomics* 54:116–123.
21. Koike C, et al. (2007) The functional analysis of TRPM1 in retinal bipolar cells. *Neurosci Res* 58 (Suppl 1):S41.
22. Bellone RR, et al. (2008) Differential gene expression of TRPM1, the potential cause of congenital stationary night blindness and coat spotting patterns (LP) in the Appaloosa horse (Equus caballus). *Genetics* 179:1861–1870.
23. Shen Y, et al. (2009) A transient receptor potential-like channel mediates synaptic transmission in rod bipolar cells. *J Neurosci* 29:6088–6093.
24. Nawy S, Jahr CE (1990) Suppression by glutamate of cGMP-activated conductance in retinal bipolar cells. *Nature* 346:269–271.
25. Wilson M, Tessier-Lavigne M, Attwell D (1987) Noise analysis predicts at least four states for channels closed by glutamate. *Biophys J* 52:955–960.
26. Xu XZ, Moebius F, Gill DL, Montell C (2001) Regulation of melastatin, a TRP-related protein, through interaction with a cytoplasmic isoform. *Proc Natl Acad Sci USA* 98:10692–10697.
27. Asano T, Semba R, Ogasawara N, Kato K (1987) Highly sensitive immunoassay for the alpha subunit of the GTP-binding protein go and its regional distribution in bovine brain. *J Neurochem* 48:1617–1623.
28. Saitoh O, Kubo Y, Miyatani Y, Asano T, Nakata H (1997) RGS8 accelerates G-protein-mediated modulation of K+ currents. *Nature* 390:525–529.
29. Ueda Y, Iwakabe H, Masu M, Suzuki M, Nakanishi S (1997) The mGluR6 5′ upstream transgene sequence directs a cell-specific and developmentally regulated expression in retinal rod and ON-type cone bipolar cells. *J Neurosci* 17:3014–3023.
30. Dryja TP, et al. (2005) Night blindness and abnormal cone electroretinogram ON responses in patients with mutations in the GRM6 gene encoding mGluR6. *Proc Natl Acad Sci USA* 102:4884–4889.
31. Niwa H, Yamamura K, Miyazaki J (1991) Efficient selection for high-expression transfectants with a novel eukaryotic vector. *Gene* 108:193–199.
32. Koike C, et al. (2005) Function of atypical protein kinase C lambda in differentiating photoreceptors is required for proper lamination of mouse retina. *J Neurosci* 25: 10290–10298.
33. Deng C, Wynshaw-Boris A, Zhou F, Kuo A, Leder P (1996) Fibroblast growth factor receptor 3 is a negative regulator of bone growth. *Cell* 84:911–921.
34. Matsui K, Hasegawa J, Tachibana M (2001) Modulation of excitatory synaptic transmission by GABA(C) receptor-mediated feedback in the mouse inner retina. *J Neurophysiol* 86:2285–2298.
35. Ghosh KK, Bujan S, Haverkamp S, Feigenspan A, Wässle H (2004) Types of bipolar cells in the mouse retina. *J Comp Neurol* 469:70–82.
36. Berntson A, Taylor WR (2000) Response characteristics and receptive field widths of on-bipolar cells in the mouse retina. *J Physiol* 524:879–889.
37. Euler T, Masland RH (2000) Light-evoked responses of bipolar cells in a mammalian retina. *J Neurophysiol* 83:1817–1829.
38. Berlin JR, Bassani JW, Bers DM (1994) Intrinsic cytosolic calcium buffering properties of single rat cardiac myocytes. *Biophys J* 67:1775–1787.

Multicenter Survey with a Systematic Overview of Acute-Onset Endophthalmitis after Transconjunctival Microincision Vitrectomy Surgery

YUSUKE OSHIMA, KAZUAKI KADONOSONO, HIDETAKA YAMAJI, MAKOTO INOUE, MUNENORI YOSHIDA, HIDEYA KIMURA, MASAHITO OHJI, FUMIO SHIRAGA, AND TOSHIMITSU HAMASAKI, ON BEHALF OF THE JAPAN MICROINCISION VITRECTOMY SURGERY STUDY GROUP

• PURPOSE: To explore the incidence and visual outcomes of acute-onset endophthalmitis after transconjunctival microincision vitrectomy surgery (MIVS).

• DESIGN: Retrospective, interventional, multicenter survey with a systematic review.

• METHODS: A clinical database search was performed at 27 institutions involving 43 868 consecutive patients who underwent vitrectomy between November 2003 and October 2008 to identify all patients with endophthalmitis after vitrectomy. A systematic review of studies reporting the endophthalmitis rates after MIVS versus 20-gauge vitrectomy was conducted to assess the pooled incidence rates of postvitrectomy endophthalmitis.

• RESULTS: The endophthalmitis rates from the multicenter survey were 0.034% (10 cases per 29 030 eyes) after 20-gauge vitrectomy and 0.054% (8 cases per 14 838 eyes) after MIVS, with no significant ($P = .603$) differences between groups. Although the incidence in 25-gauge cases (6 per 8238 eyes; 0.073%) was greater than in 23-gauge cases (2 per 6600 eyes; 0.030%), the difference was not significant ($P = 0.451$). Of 8 eyes in which endophthalmitis developed after MIVS, 6 eyes (75%) had a final visual acuity of 0.5 or better, and none lost light perception. By combining the results of 7 studies, including the current multicenter survey, meta-analyses from a total of 77 956 cases at the baseline showed that the pooled endophthalmitis rates after MIVS (0.08%; 95% confidence interval, 0.030% to 0.164%) and after 20-gauge vitrectomy (0.030%; 95% confidence interval, 0.012% to 0.048%) did not differ significantly ($P = .207$, pooled risk difference; 0.0005 [95% confidence interval, −0.0002 to 0.0012]).

• CONCLUSIONS: The incidence of postvitrectomy endophthalmitis was low with no significant differences between MIVS and 20-gauge vitrectomy. (Am J Ophthalmol 2010;150:716–725. © 2010 by Elsevier Inc. All rights reserved.)

Accepted for publication June 2, 2010.

From the Departments of Ophthalmology (Y.O.) and Biomedical Statistics (T.H.), Osaka University Medical School, Suita, Japan; the Department of Ophthalmology, Yokohama City University Medical Center, Yokohama, Japan (K.K.); the Department of Ophthalmology, Kagawa University Faculty of Medicine, Kagawa, Japan (H.Y., F.S.); the Kyorin Eye Center, Kyorin University School of Medicine, Mitaka, Japan (M.I.); the Department of Ophthalmology and Visual Science, Nagoya City University Graduate School of Medical Sciences, Nagoya, Japan (M.Y.); Nagata Eye Clinic, Nara, Japan (H.K.); and the Department of Ophthalmology, Shiga University of Medical Science, Shiga, Japan (M.O.).

Members of the Japan Microincision Vitrectomy Surgery Study Group participating in this study appear in Appendix.

Inquiries to Yusuke Oshima, Department of Ophthalmology, Osaka University Medical School, Room E7, 2-2 Yamadaoka, Suita, 565-0871, Japan; e-mail: yusukeoshima@gmail.com

ACUTE-ONSET POSTVITRECTOMY ENDOPHTHALMITIS is uncommon but remains one of the most serious complications associated with devastating visual loss or blindness, despite appropriate treatment.[1–3] The reported incidence of infectious endophthalmitis after conventional 20-gauge vitrectomy has decreased to 0.03% to 0.05% during the past decades because of improved surgical techniques and recognition of the importance of perioperative antiseptic preparations.[4–6] However, because of the recent trend toward more frequent use of and expanding indications for microincision vitrectomy surgery, there is a growing concern that microincision vitrectomy surgery with either 23- or 25-gauge instrumentation may increase the risk of postoperative endophthalmitis compared with conventional 20-gauge vitrectomy because of the transconjunctival approach and sutureless nature of the procedure.[7]

Based on a computerized search of PubMed (National Library of Medicine) databases from 2002 when modern microincision vitrectomy surgery began to be performed,[8,9] acute-onset infectious endophthalmitis after microincision vitrectomy surgery first was reported in 2005 in a case treated with a 25-gauge system,[10] and this was followed by an increasing number of small case series describing the potential risk over the years.[11–13] To date, several studies have reported the incidence of acute-onset endophthalmitis after transconjunctival 23- or 25-gauge microincision vitrectomy surgery compared with that after conventional 20-gauge vitrectomy.[14–20] However, the reported incidence of acute-onset endophthalmitis after microincision vitrectomy surgery varies across studies (0% to 1.55%), because most reports are based on the experience of individual institutions or groups of surgeons and because

0002-9394/$36.00
doi:10.1016/j.ajo.2010.06.002

statistically valid data often are limited by small sample sizes. Although a prospective, randomized, controlled study clearly would be most valid for determining the accurate incidence rates of endophthalmitis after microincision vitrectomy surgery compared with conventional 20-gauge vitrectomy, the relative rarity of endophthalmitis poses a significant challenge when conducting such a clinical trial because extraordinarily large numbers of patients (no fewer than 30 000 per group) would be required for robust data in prospective studies, given the low incidence rates.[21] In contrast, as evidenced in the postcataract endophthalmitis literature,[22] other appropriate methods, such as a systematic review of studies or a multicenter survey, are more practical and can identify the clinical and statistical trends of this devastating complication.

In the current study, we conducted a multicenter survey and a systematic overview of the recent literature and combined the results of multiple studies to obtain the best available perspective of the recent trends in acute-onset endophthalmitis after microincision vitrectomy surgery. The clinical features, management strategies, causative organisms, and visual outcomes in patients in whom acute-onset endophthalmitis developed after microincision vitrectomy surgery were investigated.

METHODS

• A RETROSPECTIVE, MULTICENTER SURVEY OF ACUTE-ONSET POSTVITRECTOMY ENDOPHTHALMITIS: A retrospective database search was performed at 27 institutions (Appendix) in Japan to identify all patients who underwent conventional 20-gauge pars plana vitrectomy (PPV) or transconjunctival microincision vitrectomy surgery with 23- or 25-gauge instruments between January 1, 2004, and December 31, 2008, and subsequently were treated for acute-onset infectious endophthalmitis after the initial vitrectomy. The time chosen for a database search was immediately after the introduction of a 25-gauge transconjunctival microincision vitrectomy surgery system in Japan. The search combined the procedure key words of *pars plana vitrectomy* with the diagnosis key word of *endophthalmitis* and specified by checking that the date of development of endophthalmitis was within 6 weeks after the date of vitrectomy. The patients' medical records were reviewed to reconfirm that endophthalmitis was associated with vitrectomy and to collect clinical data to meet the study objectives. The exclusion criteria were a preoperative diagnosis of current intraocular infection or inflammation, such as endogenous endophthalmitis, acute retinal necrosis, cytomegalovirus retinitis, and vitreous opacity associated with uveitis of unknown cause or suspicious malignancy.

In the current multicenter survey, retina specialists performed all surgeries (n = 31) in the 27 institutions after standardized preoperative antiseptic preparation that included topical administration of a third- or fourth-generation fluoroquinolone 3 to 4 times daily beginning 3 days before surgery. After scrubbing the eyelids and periorbital area with 1.25% povidone–iodine solution, undiluted povidone–iodine solution was used to sterilize the surgical field. All patients were draped in the standard fashion with the lashes everted from the surgical field. No antibiotic irrigation or intravitreal antibiotics were used during surgery. At the end of surgery, subconjunctival antibiotics, a steroid, or both were administered at the discretion of the surgeon. A topical antibiotic ointment was applied, and the eye was patched and shielded. Patients routinely received postoperative topical fluoroquinolone and prednisolone acetate for at least 1 month.

In eyes undergoing conventional 20-gauge 3-port vitrectomy, all sclerotomies were created with the 20-gauge microvitreoretinal blade after conjunctival peritomy. At the end of surgery, all 20-gauge sclerotomies and conjunctival incisions were sutured. In contrast, all sclerotomies in eyes undergoing microincision vitrectomy surgery were created transconjunctivally using 23- or 25-gauge trocar–cannula system (Alcon Laboratories, Inc, Fort Worth, Texas, USA; Dutch Ophthalmic Research Center, Zuidland, The Netherlands). The 25-gauge sclerotomies were performed using perpendicular incisions in the early years after the introduction of the 25-gauge system and then with an oblique incision from 2005 onward,[23,24] whereas the 23-gauge sclerotomies were created by an oblique incision from the time the procedure was introduced.[25] The conjunctiva was displaced before the trocar–cannula was inserted in most cases to misalign the conjunctival and scleral incisions.[9,26] All cannulas were removed at the end of surgery. The sclerotomies were sutured if the operating surgeon suspected that a leak was present.

Acute-onset postoperative endophthalmitis was defined by the presence of anterior chamber inflammatory cells with fibrin formation, hypopyon, vitreous cells and fibrin, progressive ocular pain, conjunctival congestion, and blurred vision occurring within 6 weeks after surgery.[5,14,19,27] Specimens from the vitreous biopsy were cultured, but the results were unnecessary for diagnosis of acute postoperative endophthalmitis, given the reported high false-negative rate of intravitreal sampling.[27] Data collected from the patients with acute-onset endophthalmitis included demographic information, presenting signs and symptoms, duration of symptoms, presenting visual acuity (VA), surgical details, therapeutic interventions, and postoperative course, including intraocular pressure on the first postoperative day, culture results, and VA outcomes.

• STUDY SEARCH AND SELECTION FOR META-ANALYSIS: All studies published in the English literature on endophthalmitis after 23- or 25-gauge microincision